Mesothelin secretion by pancreatic cancer cells co-opts macrophages and promotes metastasis

Teifion Luckett[1], Maidinaimu Abudula[1], Lucy Ireland[1], Mark Glenn[1], Gaia Bellomo[1], Ruth Stafferton[1], Chris Halloran[1], Paula Ghaneh[1], Rob Jones[2], Michael C. Schmid[1], Ainhoa Mielgo[1*]

[1] Department of Molecular and Clinical Cancer Medicine, University of Liverpool, Ashton Street, Liverpool, L69 3GE, UK.

[2] Department of Hepatobiliary Surgery, Liverpool University Teaching Hospitals NHS Foundation Trust, Prescot Street, Liverpool L7 8YE, UK

***Corresponding Author:** Ainhoa Mielgo, Department of Molecular and Clinical Cancer Medicine, University of Liverpool, Ashton Street, Liverpool, L69 3GE, UK. Phone: +44 151 794 9555; email: amielgo@liverpool.ac.uk

Running Title: Mesothelin regulates macrophage function and PDAC metastasis

Key words: macrophages, mesothelin, metastasis, pancreatic ductal adenocarcinoma, PDAC, pancreatic cancer, VEGFA, S100A9

Conflict of Interest Statement: A. Mielgo grants from North West Cancer Research and grants from Wellcome Trust during the conduct of the study; grants from North West Cancer Research outside the submitted work. C Halloran reports grants from Pancreatic cancer UK, grants from NHS England, and grants from Cancer Research UK outside the submitted work. No disclosures were reported by the other authors.

Abstract

Pancreatic ductal adenocarcinoma (PDAC) is a highly metastatic disease, yet effective treatments to inhibit PDAC metastasis are lacking. The rich PDAC tumor microenvironment plays a major role in disease progression. Macrophages are the most abundant immune cell population in PDAC tumors and can acquire a range of functions that either hinder or promote tumor growth and metastasis. Here, we identified that mesothelin secretion by pancreatic cancer cells co-opts macrophages to support tumor growth and metastasis of cancer cells to the lungs, liver, and lymph nodes. Mechanistically, secretion of high levels of mesothelin by metastatic cancer cells induced the expression of VEGFA and S100A9 in macrophages. Macrophage-derived VEGFA fed back to cancer cells to support tumor growth, and S100A9 increased neutrophil lung infiltration and formation of neutrophil extracellular traps. These results reveal a role for mesothelin in regulating macrophage functions and interaction with neutrophils to support PDAC metastasis.

Statement of significance

Mesothelin secretion by cancer cells supports pancreatic cancer metastasis by inducing macrophage secretion of VEGFA and S100A9 to support cancer cell proliferation and survival, recruit neutrophils, and stimulate neutrophil extracellular trap formation.

Introduction

Pancreatic ductal adenocarcinoma (PDAC) has a high propensity for metastasis and 62% of all PDAC diagnoses are made once the tumor has metastasized (1). This is in part due to late diagnosis but also the early progression to metastatic disease and the poor response to current standard care of treatments (2). Only 15% of patients have no metastatic or locally advanced disease at the time of diagnosis and are therefore eligible for surgical resection. However, many of these patients relapse due to the presence of clinically undetectable micro-metastases at the time of surgery (3,4). The 5-year survival

rate for those having undergone resection with adjuvant chemotherapy is only 21% (5) and approximately 66% will have extensive distant metastasis at the time of death (2,6,7). Pre-malignant circulating pancreatic epithelial cells can be detected as early as inflammatory PanIN pre-cursor lesions, which then gain competency for metastatic colonization upon malignant transformation (8). The liver is the most frequent site of PDAC metastasis (75-94%), however many tumors metastasize to the lungs (47-71%), lymph nodes (41-57%) and peritoneum (41-71%) (7,9). The dismal prognosis of PDAC patients highlights the need to better understand the drivers of metastatic disease in order to develop more effective therapies for pancreatic cancer.

PDAC tumors are comprised of tumor nests surrounded by a dense poorly vascularized desmoplastic stroma (10). Tumor associated macrophages (TAMs) are the most abundant immune cell population in PDAC tumors and engage in complex interactions with acellular and cellular components of the tumor microenvironment (TME) to shape tumor progression and metastasis (11-13). TAMs are a highly plastic heterogeneous cell population and acquire a range of phenotypes and functions in response to environmental cues and stimuli (14). In established PDAC tumors, infiltrated macrophages are predominantly tumor promoting and downregulate antigen presenting molecules but upregulate angiogenic factors and growth factors, fibrotic mediators, matrix remodeling enzymes and immunosuppressive signaling molecules, all of which promote tumor growth and metastasis (11,12,15-18).

PDAC metastasis is considered to be an inefficient process because less than 0.01% of disseminated cancer cells are estimated to develop into metastases (3,8). Therefore, the formation of a hospitable metastatic niche is considered to be a rate limiting step in the metastatic cascade (19). Emerging evidence has highlighted how tumor secreted factors can co-opt stromal and immune cells in the liver and lungs, to ready the metastatic site for colonization by circulating tumor cells (20-22). Inflammation provoked by the primary tumor and/or stromal mediators at the metastatic site leads to the accumulation of metastasis

promoting myeloid cells within the lung and liver pre-metastatic niche, in several cancer types (23-26). Myeloid cells further adapt the pre-metastatic niche for colonization by disseminated cancer cells, by inducing fibrosis and creating an immunosuppressive environment (13,18). Taken together, these studies underline the importance of immune cells, and notably myeloid cells, in supporting successful cancer metastasis.

Targeting the pro-metastatic functions of the TME represents an attractive treatment strategy for PDAC patients and we and others have identified stroma-derived factors promoting pancreatic cancer metastasis (13,16,18,21,22). However, why some pancreatic tumors metastasize more than others is still poorly understood. In this study, we sought to unveil mechanisms that drive PDAC metastasis, in order to identify novel therapeutic targets to treat this lethal disease.

Materials and Methods

Cells

The FC1199 and FC1245 pancreatic cancer cell lines were generated in the Tuveson lab using tumor tissues from the *Kras*^{G12D}*Trp53*^{R172H}*Pdx1-Cre* (KPC) mice of a pure C57BL/6 genetic background. Lentiviral transduction was performed using the pHIV-zsGreen-Luciferase plasmid (a gift from B. Welm; RRID:Addgene_39196) to produce the FC1199$^{zsGreen/Luc}$ and FC1245$^{zsGreen/Luc}$ cell lines, simply referred to as FC1199 and FC1245 throughout this manuscript. All cell lines were regularly tested for mycoplasma (Chembio #25235). Cells were cultured with DMEM + 10% FBS + 1% antibiotic/antimycotic solution (A5955, Sigma Aldrich) at 37˚C and 5% CO_2 and used for no more than 20 passages.

In vivo studies

C57BL/6 mice were purchased from Charles River Laboratories and housed under specific-pathogen free conditions at the Biomedical Services Unit at the University of Liverpool. All animal experiments were performed on 6-8-week-old female mice in accordance with current UK legislation under the approved project license (P16F36770).

Mice were housed under specific pathogen-free conditions at the Biomedical Science Unit at the University of Liverpool.

Low passage number $2x10^5$ FC1199, FC1245, FC1245^{Cas9} WT, FC1245$^{Msln-/-}$ #4 or #6 cells were orthotopically implanted in 30 µl of matrigel (VWR, #734-0269) into the pancreas of immunocompetent syngeneic mice using a Hamilton syringe, and grown for 20 days. Tumors, livers, lungs and tumor draining mesenteric lymph nodes were harvested at day 20. Metastasis quantification was performed *ex vivo* by coating the tissues in 100ul of 15mgml beetle luciferin (E6551, Promega) and assessing the subsequent bioluminescent signal produced by the KPC-derived$^{luc/zsGreen}$ cells (Perkin Elmer, RRID:SCR_020397) as previously described (22). Total flux [photons/sec] was quantified using the Living Image software v4.5 (Perkin Elmer; RRID:SCR_014247).

Generation of conditioned media

Tumor conditioned media (TCM) was generated by seeding $2x10^6$ KPC-derived cells into a T75 flask and growing them until they reach 70-80% confluence. Cells were then washed 3x with PBS and cultured with serum free DMEM for 24-36hours. The conditioned media was harvested, centrifuged and the supernatant put through a 0.45µM filter to remove dead cells and debris.

Primary macrophages were generated by flushing the bone marrow from the tibia and femur of C57BL/6 mice, followed by density centrifugation and cultured with 10ng/ml of m-csf (315-02, Peprotech) in DMEM + 10% FBS in a 10cm dish ($20x10^6$ cells) for 5 days. At day 5, m-csf was removed and non-adherent cells washed off. At day 6 tumor conditioned media was added to the macrophages with 2% FBS and cultured for 24-36hrs. The resulting Tumor educated Macrophage Conditioned Media (TeMCM) was collected, centrifuged and put through a 0.45µM filter to remove dead cells and debris.

Proteomic analysis

The FC1199 and FC1245 cells were cultured with R6K6 and R0K0 non-phenol red serum free SILAC media respectively for 24hrs. The supernatant was then harvested, centrifuged and passed through a 0.22µM filter. This procedure was performed in quadruplet to produce 4 replicates. The SILAC TCM from each replicate was concentrated onto 10µl of strataclean beads (Agilent Technologies Inc.) and washed twice with 25mM ammonium bicarbonate. The resin beads were resuspended in 80µl of 25mM ammonium bicarbonate and 5µl 1% (w/v) Rapigest™ (Waters). The samples were denatured at 80˚C for 10 minutes, reduced with 5µl of 60mM Dithiothreitol (DTT) at 60˚C for 10 minutes, cooled and alkylated with 5µl of 180mM iodoacetamide. The samples were incubated with 1µg of porcine sequencing grade trypsin (Promega, #V511A) overnight on a rotary mixer at 37˚C. Afterwards, the digests were acidified with Trifluoroacetic acid for 45 minutes at 37˚C to remove Rapigest™ surfactant. Samples were centrifuged at 17000g for 30 minutes and 10µl of each supernatant was taken for liquid chromatography tandem mass spectrometry using a QExactive HF quadruple-Orbitrap mass spectrometer (RRID:SCR_020556) coupled to a Dionex Ultimate 3000 RSLC nano-liquid chromatograph (Thermo Fisher). Separation was performed using a 120minute gradient, with the eluent being introduced to the integrated nano-electron spray ionization source operating in positive ion mode.

The raw mass spectra were searched against the Mus Musculus UniprotKb FASTA protein sequences (accessed July 2020) using MaxQuant (v1.6.8, RRID:SCR_014485) with the Andromeda peptide search engine with the false discovery rate set to 0.01. MaxQuant output ratios were filtered to remove contaminants, peptides not present in every replicate and proteins identified by only 1 peptide. The FASTA sequences of all differentially secreted or exclusively secreted proteins were assessed for prediction of classical secretion using Secretome P v5.0 (NN-score >0.05), Signal P v5.0 (p>0.9) and Target P v2.0 (p>0.9). The proteins were filtered for possession of multiple transmembrane helices using TMHMM v2.0 (RRID:SCR_014935). Proteins were also checked for exosomal or vesicular secretion using Exocarta (RRID:SCR_021960) and Vesiclepedia databases

(RRID:SCR_019011). Differentially secreted proteins were identified using the LIMMA package (Ritche *et. al* 2015, RRID:SCR_010943) in 'R' (v4.1.3) using empirical bayes moderation. Log2 fold change and p value cut off's applied were 1.25 and 0.01 respectively. The genes of the remaining proteins with human orthologues were used for Kaplan Meier survival analysis ('survminer' package v3.3-1 in 'R') using the Pancreatic Adenocarcinoma dataset (PAAD) from The Cancer Genome Atlas (TCGA). PAAD TCGA samples were stratified to include only PDAC cases as previously described (27).

The mass spectrometry proteomics data have been deposited to the ProteomeXchange Consortium via the PRIDE (28) partner repository with the dataset identifier PXD042234.

Flow cytometry analysis

Single cell suspensions of PDAC tumor and lungs were prepared by first mechanically disrupting the tissues, followed by enzymatic digestion in Hanks Balanced Salt Solution supplemented with 1mg/ml of Collagenase P (for PDAC tumors) or 2mg/ml of Collagenase D (Lungs) for 30 minutes at 37˚C. The cell suspensions were further digested in TrypPLE (Thermofisher) for 5mins at 37˚C and subsequently filtered 70µm cell strainer to obtain a single cell suspension. Red blood cell lysis was performed and the samples were blocked with 1:100 of Fc Block (BD Pharmingen, #553142, RRID:AB_394657) for 10 minutes on ice. The cells were then incubated with SYTOX™ Blue (Thermofisher, #S11348) and conjugated antibodies against CD45 (Biolegend, #103116, RRID:AB_312981), F4/80 (Biolegend, #123115 RRID:AB_893493), MHC class II (Biolegend, #107630, RRID:AB_2069376), Ly6G (Biolegend, #127618, RRID:AB_1877261) and Ly6C (Biolegend, #128008, RRID:AB_1186132). Flow cytometry analysis was performed on FACS Canto II (RRID:SCR_018056).

CRISPR/Cas9 knockout of Mesothelin in the FC1245 cells and rescue of mesothelin expression

Lentivirus was produced by transfecting a 10-cm dish containing HEK293T cells at ~80% confluence with pCW-Cas9 (a gift from E. Lander and D. Sabatini; RRID:Addgene_50661), together with the helper plasmids psPAX2 (RRID:Addgene_12260) and pMD2.G (RRID:Addgene_12259) vectors at a 1:4:2 ratio using polyethyleneimine. The pCW-Cas9 plasmid contains a TET operator for doxycycline inducible expression of SpCas9. After 72 hours, the supernatant was collected and centrifuged at 500*g* for 5 minutes to remove cell debris. The clarified supernatant was filtered using a 0.45-µm PVDF filter and used to transduce FC1245 cells. Successfully transduced FC1245^{SpCas9} clones were isolated and validated by western blotting. sgRNA plasmids targeting two separate sites within *Msln* were constructed by ligating annealed oligonucleotides containing the desired spacers into BsmBI digested pMuLE ENTR U6 L1-R5 (a gift from I. Frew; RRID:Addgene_62111). We next transfected the gRNA vectors into FC1245^{SpCas9} cells using lipofectamine 2000 (Thermo Fisher, #11668019). SpCas9 expression was induced the following day through addition of 8ug/ml of doxycycline. Successfully transfected single cell clones were isolated and screened for homozygous deletion by PCR. Sequences of oligonucleotides used to generate sgRNA and primers used for genetic validation of the knockout clones can be found in Supplementary Table S1.

We later rescued mesothelin expression in the FC1245$^{Msln-/-}$ #4 cells by performing lentiviral transduction using a lentiviral vector containing genes for *Msln* expression and blasticidin resistance (pHIV-Msln-BSD plasmid). The procedure for lentivirus production and transduction is the same as described above. Blasticidin antibiotic selection was carried out at 5nM for 14 days to generate the 'FC1245$^{Msln-/-}$ + *Msln'* cell line.

Colony formation assay

Each well of a 48 well plate was coated with a melted 0.5% (w/v) agarose solution made with non-phenol red DMEM and allowed to set. Either FC1199, FC1245 or FC1245$^{Msln-/-}$ cell suspensions were put through a 70µM filter and seeded at 3000 cells per well in a melted 37°C 0.3% (w/v) agarose solution made with either DMEM, FC1199 TeMCM,

FC1245 WT TeMCM, FC1245 WT (*Cas9*) TeMCM, or FC1245$^{Msln-/-}$ TeMCM, supplemented with 4% FBS. After the cell containing layer had set, TeMCM was layered on top, supplemented with 4% FBS and changed every 2-3 days until day 11. For VEGFR2 inhibition experiments 50mM of Ki8751 (Selleckchem, #S1363) or dimethyl sulphide (DMSO) control vehicle was added to the cell layer and feeder layer. For VEGFA stimulation experiments, 150nM of recombinant VEGFA (Biolegend, #583104) was used at 150nM in the cell layer and feeder layer. Colony formation was quantified after 11 days by administering beetle luciferin (15mg/ml) and measuring the bioluminescent signal by IVIS. Representative brightfield images of the colonies were also produced.

MTT proliferation assay

2,000 FC1199 or FC1245 cells were seeded into a 96 well plate in non-phenol red DMEM + 10% FBS. Cell proliferation was assessed at 0, 24 and 48hrs using the CyQuant MTT cell proliferation assay kit (Thermofisher) according to the manufacturer's instructions.

Immunoblotting

Immunoblotting for secreted proteins was performed by concentrating proteins from the conditioned media onto Strataclean resin beads (Agilent Technologies). Loading buffer (187.5mM Tris base, 9 % Sodium Dodecyl Sulfate (SDS), 10 % β-mercaptoethanol, 30 % glycerol and 0.05 % bromophenol blue) was added to the beads in a 1:1 ratio and heated for 10 minutes at 95˚C. For immunoblotting of membrane bound proteins, cells were scraped and lysed on ice with RIPA buffer (50 mM Tris, pH 7.4, 150 mM NaCl, 1% Triton X-100 and 0.1% SDS) supplemented with HALT protease and phosphatase inhibitor cocktail (Thermo Fisher, #78429), 100mM PMSF (Sigma Aldrich, #P7626) and 100mM sodium orthovanadate (Sigma Aldrich, #S6508). Protein concentration was determined using the Pierce BCA assay kit (Thermo Fisher, #23225). Loading buffer was added to the lysates and heated for 10 minutes at 95˚C. Beads and lysates were loaded into a SDS-PAGE gel for electrophoresis. Proteins were transferred onto a PVDF membrane, blocked

with 5% BSA, then incubated with the following antibodies: Msln 1:1000 (IBL, #28127 RRID:AB_2341524), VEGFR2 1:200 (R&D Systems, RRID:AB_355500) phosphorylated-VEGFR2 (Cell Signaling Technologies, #2478, RRID:AB_331377), α-Tubulin 1:10000 (Sigma Aldrich, #T6199, RRID:AB_477583), SpCas9 1:1000 (Cell Signaling Technologies, #65832, RRID:AB_2799695), GPI-PLD 1:500 (Abcam, #ab210753). Secondary anti-rabbit (Cell Signaling Technologies, #7074, RRID:AB_2099233) or anti-mouse HRP antibodies (Cell Signaling Technologies, #7076, RRID:AB_330924) and imaged using SuperSignal™ West Pico PLUS (Thermo Fisher, #34580).

Immunohistochemistry

Formalin fixed paraffin embedded tissue sections were deparaffinized using the DAKO PT link and treated with DAKO peroxidase blocking solution (Agilent, S202386-2). Sections were incubated with primary antibodies overnight at 4˚C: α-smooth muscle actin 1:200 (Abcam, #ab5694, RRID:AB 2223021), NKp46 1:50 (R&D Systems, #AF2225, RRID:AB_355192), CD31 1:100 (Cell Signaling Technology, #77699, RRID:AB_2722705). The sections were then incubated with DAKO anti-rabbit HRP labelled polymer (K4003, Agilent) or Donkey anti-goat HRP 1:250 (Abcam, #ab97051, RRID:AB_10679369) secondary antibodies for 30 minutes at room temperature. Immunostaining was visualized using Dako Liquid DAB+ Substrate Chromogen System (K3468, Agilent) and counterstained with hematoxylin.

Immunofluorescence in FFPE tissues

Formalin fixed paraffin embedded tissue sections were deparaffinized using the DAKO PT link. Sections were permeabilised using 0.1% triton X-100 in PBS and blocked with donkey serum. The following primary antibodies were incubated overnight at 4˚C: CK19 1:500 (ab133496, Abcam), Ki67 1:100 (#14-5698-80, Thermo Fisher), F4/80 1:100 (70076T, Cell Signaling Technology, #77699, RRID:AB_2722705), F4/80 1:50 (Biolegend, #123101, RRID:AB_893504), CD206 1:1000 (Abcam, #ab64693, RRID:AB_1523910), MHC II 1:100

(Novus Biologicals, #NBP1-43312, RRID:AB_10006678), Arginase1 (Proteintech Group, 16001-1-AP, RRID:AB_2289842), Vascular Endothelial Growth Factor Alpha 1:25 (Santa Cruz, #SC-7269, RRID:AB_628430), S100A9 1:2000 (Novus Biologicals, NB110-89726, RRID:AB_1217846), CD8a 1:50 (Thermo Fisher, #14-0808-82, RRID:AB_2572861), CD4 1:50 (Thermo Fisher, #14-9766-80, RRID:AB_2573007), Granzyme B 1:100 (ab4059, Abcam, #ab4059, RRID:AB_304251), FOXP3 1:100 (Cell Signaling Technology, #12653S, RRID:AB_2797979), Ly6G (Biolegend, 127602, RRID:AB_1089180), anti-human VEGFR2 1:2000 (Cell Signaling Technology, #2479, RRID:AB_2212507), pan-keratin 1:250 (Cell Signaling Technology, #4545, RRID:AB_490860). The next day, sections were washed with PBS and incubated with 5mg/ml 4′,6-diamidino-2-phenylindole (DAPI) and fluorescently labelled secondary antibodies for 2hrs at room temperature: Donkey anti-rat AF488 1:300 (ab150149, Abcam), Donkey anti-rat AF647 1:300 (ab150155, Abcam), Donkey anti-rabbit AF488 1:200 (406416, Biolegend), Donkey anti-rabbit AF594 1:200 (406415, Biolegend), Donkey anti-rabbit AF647 1:200 (406414, Biolegend), Donkey anti-mouse AF594 (ab150112, Abcam). Sections were mounted onto coverslips using Dako Fluorescent mounting medium (S302380-2, Agilent). Slides were imaged using Axio Observer Light Microscope with the Apotome.2 (Zeiss). Positive cells were counted manually (using 3-8 field of view per sample) whereas cell nuclei counting was automated using QuPath (v0.2.3, RRID:SCR_018257).

Picrosirius red staining

FFPE tumor sections were deparaffinized in xylene and rehydrated through decreasing concentration of alcohol. The slides were washed in distilled H_2O and submerged in 0.2% phosphomolybdic acid for 5 minutes. The slides were then washed with PBS and submerged in 0.1% Picrosirius Red solution made with picric acid for 90 minutes. After washing in 0.5% glacial acetic acid, the slides were stained in 0.0166% Fast green FCF solution made up in 0.5% glacial acetic acid. After one more wash in 0.5% glacial acetic acid the slides were immediately dehydrated 100% ethanol, cleaned through xylene and

mounted onto coverslips using DPX new mounting media (1.00579, Sigma Aldrich). Slides were scanned and Picrosirius red staining was quantified in ImageJ (v1.5.3, RRID:SCR_003070).

Quantitative real-time PCR

Total RNA was isolated from cancer cells and macrophages using RNeasy kit (74106, Qiagen) and checked for quality and quantity using Nanodrop spectrophotometer. Reverse transcription of 500ng total RNA was performed using MMLV reverse transcriptase (28025013, Thermo Fisher) according to the manufacturer's instructions. Quantitative PCR was performed using 5x HOT FIREPol EvaGreen qPCR Mix Plus ROX (08-24-00020, Solis Biodyne) on the MX3005P RT-PCR system (Agilent). The following Quantitect Primer Assays (Qiagen) were used to assess mRNA levels: *Snail1* (Mm_Snai1_1_SG, QT00240940), *Snail2* (Mm_Snai2_1_SG, QT00098273), *Twist1* (Mm_Twist1_1_SG, QT00097223), *Twist2* (Mm_Twist2_1_SG, QT00101598), *Zeb1* (Mm_Zeb1_1_SG, QT00105385), *Zeb2* (Mm_Zeb2_1_SG, QT00148995), *Cdh1* (Mm_Cdh1_1_SG, QT00121163), *Ctnnb1* (Mm_Catnb_1_SG, QT00160958), *Epcam* (Mm_Epcam_1_SG, QT00248276), *Vim* (Mm_Vim_1_SG, QT00159670), *Cdh2* (Mm_Cdh2_1_SG, QT00148106), *Msln* (Mm_Msln_1_SG, QT00104573), *Ciita* (Mm_Ciita_1_SG, QT00153398), *Nos2* (Mm_Nos2_1_SG, QT00100275), *Tnfa* (Mm_Tnf_1_SG, QT00104006), *Il1b* (Mm_Il1b_2_SG, QT01048355), *Mrc1* (Mm_Mrc1_1_SG, QT00103012), *Arg1* (Mm_Arg1_1_SG, QT00134288), *Il6* (Mm_Il6_1_SG, QT00098875), *Chil3* (Mm_Chil3_1_SG, QT00108829), *Tgfb1* (Mm_Tgfb1_1_SG, QT00145250), *Gas6* (Mm_Gas6_1_SG, QT00101332), *Mmp9* (Mm_Mmp9_1_SG, QT00108815), *S100a9*, (Mm_S100a9_1_SG, QT00105252), *Pdcd1lg1* (Mm_Pdcd1lg1_1_SG, QT00148617), *Vegfa* (Mm_Vegfa_1_SG, QT00160769). The remaining primer sequences can be found in Supplementary Table S1. Relative expression levels were normalized to *Gapdh* expression according to the formula $2^{-\Delta}$Ct. Fold change was calculated using $2^{-\Delta\Delta Ct}$.

Statistics

Statistical analysis of experiments was performed using either unpaired student's t-test for 2 groups or one-way ANOVA with Šidák multiple comparison tests for 4 or more groups in Graphpad Prism 8 (RRID:SCR_002798) as indicated in the figure legend. Error bars represent either standard deviation or standard error as indicated in the figure legend. Standard deviation was used where the means of individual measurements are compared, whereas standard error was used where the means of biological replicates are being compared. A p-value < 0.05 was considered statistically significant.

Human tissues

Studies involving use of human PDAC tissues were approved by the University of Liverpool and National Research Ethics Service (NRES) Committee North West-Greater Manchester (REC15/NW/0477) and conducted in accordance with the Declaration of Helsinki. Human PDAC samples were obtained from patients that had given written informed consent for surplus tissue being collected for research purposes. All PDAC diagnoses were histologically confirmed by a consultant histopathologist.

Data Availability Statement

The proteomic data generated in the study are available at the ProteomeXchange Consortium via the PRIDE (28) partner repository with the dataset identifier PXD042234. Data generated in this study are included within the supplementary material. All other raw data generated in this study are available upon request from the corresponding author.

Results

Metastatic pancreatic tumors are enriched in CD206+/MHC II- macrophages

We investigated the characteristics of primary PDAC tumors and common-sites of PDAC metastasis in mice bearing tumors derived from two *Kras*^{G12D}*Trp53*^{R172H}*Pdx1-Cre* (KPC) pancreatic cancer cell lines, referred to as FC1199 and FC1245. The FC1199 and FC1245

cell lines, were stably transduced with a reporter lentivirus to express *zsGreen/luciferase* and pancreatic tumor formation was induced by orthotopic implantation of KPC-derived cancer cells into the pancreas of syngeneic immunocompetent mice (Fig. 1A). Cancer cell expression of luciferase enabled us to quantify spontaneous metastasis to the tumor draining mesenteric lymph nodes, lungs and livers. Like human PDAC, this mouse PDAC model produces fibrotic tumors that are highly infiltrated with macrophages (10,16).

We observed that the FC1245-derived tumors were significantly larger (Fig. 1B) and metastasized more to the lungs, liver and tumor draining mesenteric lymph nodes (Fig. 1C-D) than the FC1199-derived tumors. These findings suggest that despite originating from the same genetic background, the FC1199 and FC1245 cancer cells display very different tumor progression and metastatic capacity *in vivo*. To investigate whether cancer cell intrinsic mechanisms, could explain the differences in tumor growth and metastasis we assessed the proliferation and survival capacity of the FC1199 and FC1245 cells *in vitro*. Although the high metastatic (FC1245) cancer cell line had an initial proliferative advantage *in vitro* over the low metastatic (FC1199) this was lost at 48hrs (Fig. 1E). Moreover, both cell lines displayed similar levels of intrinsic growth in 3D culture (Fig. 1F) and a similar phenotype (Supplementary Fig. S1A). We also assessed epithelial mesenchymal transition (EMT) markers and observed that the high metastatic FC1245 cells had significantly less expression of the EMT inducing transcription factors *Snail1* and *Snail2* and a small but significant increase in *Cdh1* (E-cadherin) expression compared to the low metastatic FC1199 (Fig. 1G). Taken together these findings suggest that there are no major differences in proliferation, survival or EMT between the FC1199 and FC1245 cells *in vitro* that could explain the differences observed in tumor growth and metastasis *in vivo*. We then examined cancer cell proliferation and survival in the PDAC tumors. Immunofluorescent co-staining (IF) for tumor cells (cytokeratin 19+) and the proliferation marker Ki67 in PDAC tumor tissues showed no differences in cancer cell proliferation *in vivo* (Fig. 1H). However, TUNEL staining for apoptotic tumor cells showed a significant

365 decrease in apoptotic tumor cells in the FC1245-derived PDAC tumors compared to the
366 FC1199-derived tumors (Fig. 1I). Together, these data suggest that the increase in cell
367 survival of the FC1245 cells *in vivo* drives tumor growth and that this is not due to a cancer
368 cell intrinsic mechanism but requires the tumor microenvironment since the increase in
369 cancer growth and survival is only observed in tumors, *in vivo*.

370 Since fibroblasts can contribute to tumor growth and metastasis (13,18), we assessed the
371 level of fibrosis by staining for αSMA and collagen, but no significant differences were
372 detected (Supplementary Fig. S2A-B). We then investigated whether a decrease in
373 effector T cells and NK cells in the highly metastatic FC1245-derived tumors could explain
374 their increase in tumor growth and metastasis. We observed no statistically significant
375 differences in activated CD8 T cells (CD8+/Granzyme B+) in the primary tumor and lungs
376 (Supplementary Fig. S2C-D). We noted that the FC1245-derived tumors had significantly
377 reduced levels of both, effector CD4 and regulatory T cells, compared to the FC1199-
378 derived tumors in the primary PDAC tumor, but not in the lungs (Supplementary Fig. S2E-
379 F). Furthermore, there were no statistically significant differences in the levels of activated
380 NK cells, as indicated by expression of NKp46+ (Supplementary Fig. S2G). Therefore, our
381 data suggest that there are no differences in the activation of T cell and NK cell populations
382 between FC1245-derived and FC1199-derived tumors that could explain the differences
383 in tumor growth and metastasis.

384 Macrophages are the most abundant immune cell population in PDAC tumors and are
385 known to change their phenotype and function in response to environmental stimuli. In
386 tumors, macrophages often adopt tumor promoting functions and support cancer
387 progression, metastasis, resistance to therapies and inhibit the anti-tumor immune
388 response (11,13,16-18,21,22). Macrophages expressing MHC class II have been
389 demonstrated to support anti-tumor immunity in PDAC, whereas CD206+ macrophages
390 are associated with a worse prognosis and in PDAC patients (29,30). To characterize the
391 macrophages, present in the FC1199 and FC1245-derived tumors, we performed

immunofluorescent analyses of the pan-macrophage marker (F4/80) in combination with MHC class II and CD206 in order to see if differences in macrophage populations could explain the differences in metastasis we observed between the two pancreatic cancer cell lines. We also studied changes in macrophage populations in the lungs, because this is the site with the most frequent and largest metastases in this mouse model (22). We found that the macrophages from the FC1245-derived primary PDAC tumors have significantly lower expression of MHC II and higher expression of CD206 compared to the FC1199-derived PDAC tumors (Fig.1J). Immunofluorescent analysis of the lung tissues showed that the mice with FC1245 tumors had a 2-fold increase in macrophage levels compared to the FC1199 tumors (Fig. 1K). Consistent with the results from the primary PDAC tumors, the macrophages in the lungs of the mice bearing FC1245 tumors had lower expression of MHC II and higher expression of CD206, compared to the lungs from the FC1199 tumor bearing mice (Fig. 1K). Taken together this data suggest that highly metastatic FC1245 tumors are characterized by an increase in CD206+ macrophages, coupled with a loss of antigen presenting MHCII + macrophages, while fibrosis, CD8 T cells and NK cells infiltration remain similar compared to FC1199 tumors.

Metastatic pancreatic cancer cells secrete higher levels of mesothelin which correlate with an increase in CD206+ macrophages and worse prognosis in PDAC patients

Since our data show metastatic pancreatic cancer cells promote an increase in CD206+ macrophages and a decrease in MHC II+ macrophages, we hypothesized that a factor secreted by metastatic pancreatic cancer cells might regulate macrophage function to support cancer cell survival and metastasis. To identify differentially secreted factors between the low (FC1199) and high (FC1245) metastatic cancer cells we used a SILAC based proteomics approach coupled with LC/MS/MS (Fig. 2A). A total of 1195 proteins were identified in the secretome of the two cell lines across all 4 biological replicates. We then removed contaminants, proteins not present in every replicate and proteins with

multiple transmembrane helices predicted by TMHMM. Further verification of secretion was performed using prediction of secretion tools (Secretome P, Signal P, Target P) and identification of secreted proteins in the vesiclepedia and exocarta databases. Differential expression analysis of the remaining 174 secreted proteins revealed that 59 proteins were enriched or exclusive to the secretome from the low metastatic FC1199 cells, 53 were common to both and 62 were enriched or exclusive to the secretome from the high metastatic FC1245 cells (Fig. 2A-B and Supplementary Table S2-4). Next, we performed survival analysis for the genes of the proteins enriched or exclusive to the secretome of the FC1199 and FC1245 cells using The Cancer Genome Atlas (TCGA) pancreatic adenocarcinoma (PAAD) dataset. We investigated whether any of the proteins exclusively expressed or enriched in the secretome of the low metastatic FC1199 correlated with an improved prognosis but found none (Supplementary Fig. S3A). A search for proteins exclusive to or enriched in the secretome from the high metastatic (FC1245) cells that correlate with a worse prognosis in PDAC patients, identified Mesothelin (*Msln*), Methylenetetrahydrofolate dehydrogenase 1 (*Mthfd1*), Semaphorin 3C (*Sema3C*) and Semaphorin 4B (*Sema4b*) (Fig. 2C). Among the candidates identified we chose to investigate mesothelin because mesothelin correlates with the worst survival for PDAC patients (Fig. 2C and Supplementary Fig. S3B) and has been reported to regulate macrophage functions *in vitro* and peritoneal macrophage homeostasis *in vivo* (31,32). Mesothelin is a glycophosphoinositol anchored (GPI) protein whose expression is mainly limited to the mesothelium in health. However, upon malignant transformation, PDAC cells highly express mesothelin (33). Next, we validated the presence of secreted mesothelin in the tumor conditioned media (TCM) of the cancer cell lines by immunoblotting and confirmed that the high metastatic (FC1245) cancer cells secrete more mesothelin than the low metastatic (FC1199) cells (Fig. 2D). Furthermore, immunofluorescent staining for mesothelin and pan-keratin in PDAC patient tissue samples confirmed that cancer cells are the main source of mesothelin in the PDAC TME (Supplementary Fig. S4A).

Mesothelin has been reported to regulate macrophage polarization *in vitro* through the binding of the mannose residues of its GPI-anchor to the mannose receptor (CD206) on macrophages (31) and to induce an inflammation resolving macrophage phenotype in a peritoneal injury model (32). Thus, we sought to investigate whether increased secretion of mesothelin by the high metastatic (FC1245) pancreatic cancer cells co-opts macrophages in the TME to promote PDAC tumor growth and metastasis. Since GPI-anchored shed mesothelin has been reported to engage CD206 (31), we investigated the expression of GPI-specific phospholipase D (*Gpld1*), the only known mammalian enzyme reported to cleave GPI-anchored mesothelin with the terminal mannose residue intact, in the FC1199 and FC1245 cells (34). We found that the high metastatic (FC1245) cells had 4-fold higher expression of *Gpld1* mRNA compared to the low metastatic (FC1199) (Fig. 2E), and expressed more GPI phospholipase D protein (Fig. 2F). Next, we investigated whether intensity of mesothelin staining on pancreatic cancer cells correlates with increased levels of CD206+ macrophages in human PDAC tissues. We discovered that there is a positive correlation between mesothelin staining intensity on pancreatic cancer cells and CD206+ macrophages in PDAC patients (Fig. 2G-H and Supplementary Fig. S4B). Therefore, our data show that the high metastatic FC1245 cells express higher levels of mesothelin and that in PDAC patient samples, high mesothelin levels correlate with an increased number of CD206+ macrophages and poorer survival.

To further understand how the FC1245 cells regulate macrophage function, we exposed primary macrophages to tumor conditioned media (TCM) and measured expression of macrophage genes *Ciita, Cd86, Nos2, Tnfα, Il1b, Cxcl10*, *Il6*, *Mrc1, Arg1, Chil3, Tgfb1, Gas6, Mmp9, Il10, S100a8, S100a9, Pcdc1lg1* and *Vegfa*. We observed that *Cxcl10* was the only inflammatory gene that was significantly decreased in the macrophages exposed to the TCM from the high metastatic FC1245 cells compared to the TCM from the low metastatic FC1199 cells (Fig. 3A). Moreover, exposure of macrophages to high metastatic FC1245-derived factors resulted in a significant increase in the expression of *Arg1*,

S100a9 and *Vegfa* (Fig.3A and Supplementary Fig. S5A). We then sought to validate whether these differences were present in macrophages *in vivo,* in primary PDAC tumors and in lung tissues. In agreement with our *in vitro* results, the macrophages present in the FC1245-derived primary PDAC tumors and lungs showed significantly higher levels of arginase (ARG1) and vascular endothelial growth factor alpha (VEGFA) compared to the macrophages infiltrated in the FC1199-derived primary PDAC tumors and lungs (Fig. 3B-C). We found that although few macrophages expressed S100A9 in the primary PDAC tumors, there was a small but significant decrease in S100A9+ macrophages in the FC1245 tumors. Whereas in the lungs of mice bearing FC1245 tumors, there were significantly more S100A9+ macrophages (Fig. 3D). Taken together these data suggest that secretion of mesothelin by pancreatic cancer cells triggers an increase in macrophages that express significantly higher levels of arginase and VEGFA in both the primary PDAC tumor and lungs, and higher levels of S100A9 in the lungs, and this correlates with increased metastasis.

Macrophage expression of VEGFA increases cancer cell colony formation in a VEGFR2 dependent manner

Next, we aimed to investigate the mechanism(s) by which macrophage-derived VEGFA, S100A9 and arginase support pancreatic cancer progression and metastasis. Arginase is an enzyme that can be secreted by macrophages and depletes L-arginine from the TME thereby removing a crucial metabolic substrate for NK and T cell function (35,36). However, since we did not observe a change in NK cell and T cell activation in FC1245-derived tumors (Supplementary Fig. S2C-G), increased arginase expression levels do not explain the aggressive phenotype of the FC1245 tumors. Thus, we focused on the mechanisms by which macrophage derived VEGFA+ and S100A9+ could promote PDAC metastasis. VEGFA promotes endothelial cell proliferation and angiogenesis, but can also bind to VEGF receptors expressed by cancer cells to enhance their proliferation and survival (37-40). Therefore, we performed an immunohistochemical staining for the

endothelial protein CD31 to see if the increased expression of VEGFA in the high metastatic tumors results in increased angiogenesis. We observed no significant differences in micro vessel density (MVD) (Fig. 4A). Thus, we hypothesized that the increase in macrophage expression of VEGFA supports cancer cell survival and tumor growth. To test our hypothesis, we performed a cancer cell colony formation assay using the secreted media from macrophages previously exposed to the FC1199 or the FC1245 cancer cells (Fig. 4B). As expected, the macrophages exposed to the FC1245 cancer cells conferred a greater colony forming ability to both cancer cell lines compared to macrophages exposed to the FC1199 cancer cells (Fig. 4C). To demonstrate that macrophage derived VEGFA is responsible for the increase in cancer cell colony formation we repeated a similar experiment where we pharmacologically blocked VEGFA signaling. VEGFA can bind to VEGFR1 and -2 however VEGFR1 has a 10-fold lower kinase activity than VEGFR2 and is considered to act as a decoy receptor (41). We therefore used a potent selective VEGFR2 inhibitor, Ki8751, to block VEGFA signaling. We show that the addition of recombinant VEGFA (rec-VEGFA) increased phosphorylation of VEGFR2 in the FC1245 cancer cells and that this effect could be abrogated upon addition of VEGFR2 inhibitor, Ki8751 (Fig. 4D). Furthermore, addition of the VEGFR2 inhibitor reduced the colony forming ability of the FC1245 cells cultured with factors secreted by macrophages previously exposed to FC1245 cells but, as expected, had no effect on the colony forming ability of the FC1245 cells cultured with factors secreted by macrophages previously exposed to the FC1199 cells (Fig. 4E). In agreement with these findings, recombinant VEGFA increased the colony forming ability of both the low metastatic FC1199 and high metastatic FC1245 cancer cells (Fig. 4F). Taken together, the data suggest that macrophages exposed to the high metastatic FC1245 pancreatic cancer cells secrete VEGFA, which in turn binds to and activates VEGFR2 in the cancer cells resulting in enhanced cancer survival and tumor growth.

Macrophage expression of S100A9 in the lungs correlates with neutrophil recruitment and NET formation

S100A9 is a potent neutrophil chemoattractant and high levels of extracellular S100A9 (and its S100A8/A9 heterodimer) have been implicated in neutrophil recruitment, activation, degranulation, inflammatory cytokine release and NET formation (42,43). Moreover, S100A9 in the lung aids in the formation of the lung pre-metastatic niche and lung tropic metastasis (44-46). NETosis (or NET formation) is the process where decondensed chromatin and granule proteins are rapidly ejected from neutrophils to form web-like structures (43). NET formation can support lung metastasis (23,47), therefore we investigated the levels of infiltrating neutrophils and NETosis in the FC1199 and FC1245-derived tumors. We previously showed that FC1245-derived tumors showed a small but significant reduction of S100A9+ macrophages in the primary tumor, and this correlates with decrease neutrophil infiltration in the primary tumor (Fig. 4G). However, the higher levels of S100A9 macrophages in the lungs of the mice bearing FC1245 tumors correlates with high levels of neutrophil infiltration and NET formation, denoted by citrinullated histone H3 staining (Ci-H3) (Fig. 4H). These results show that macrophages in FC1245-derived lungs secrete higher levels of S100A9 and have an increased infiltration of neutrophils and NETosis.

Together, these findings suggest that metastatic pancreatic cancer cells promote the secretion of VEGFA and S100A9 by tumor associated macrophages which support tumor growth, and neutrophil infiltration and NETosis in the lungs.

Genetic depletion of mesothelin inhibits tumor growth and metastasis and restores macrophage tumor suppressing functions

In order to demonstrate whether mesothelin causes metastasis and regulates macrophage and neutrophil function, we genetically depleted mesothelin from FC1245 cells using CRISPR gene editing (Supplementary Fig. S6). We first generated a single cell cloned

552 FC1245^{Cas9} WT cell line with inducible expression of *Cas9*. Shortly after, we transiently
553 expressed the gRNA pair in the FC1245^{Cas9} WT cells to generate 10 knockout clones, of
554 which 3 displayed a homozygous deletion for *Msln* (Supplementary Fig. S6B). We selected
555 homozygous KO clones #4 and #6 to be studied further. We used the parental single cell
556 cloned FC1245^{Cas9} wildtype (WT) as an additional control, to show that phenotypic
557 differences in the knockout cells are due to depletion of mesothelin and not to effects
558 caused by clonal selection. We confirmed that there was no 'leaky' Cas9 expression in
559 unstimulated cells, since Cas9 could represent a neo-antigen and alter immune responses
560 *in vivo* (Supplementary Fig. S6C). Depletion of mesothelin was confirmed at mRNA and
561 protein level (Supplementary Fig. S6E-F). As expected this corresponded with a loss of
562 secreted mesothelin in the TCM (Fig. 5A and Supplementary Fig. 6G). While depletion of
563 mesothelin in the high metastatic FC1245 cancer cells led to a significant reduction in
564 *Twist1* expression it did not affect the expression of epithelial and mesenchymal markers,
565 nor did it affect their phenotype *in vitro* (Supplementary Fig. S7). Furthermore, depletion
566 of mesothelin did not affect the ability of cancer cells to grow in 3D mono-cultures
567 (Supplementary Fig. S7B).

568 To determine whether secreted mesothelin directly alters macrophage phenotype and
569 function we exposed macrophages to FC1245 WT, FC1245^{Cas9} WT or FC1245$^{Msln-/-}$ clones
570 #4 and #6 TCM. Macrophages exposed to TCM from FC1245$^{Msln-/-}$ cells expressed higher
571 levels of MHC II compared to macrophages exposed to TCM from WT FC1245 cells and
572 resulted in a significant increase in the ratio of MHC II+:CD206+ macrophages (Fig. 5B).

573 We then investigated how mesothelin depletion affects tumor progression, metastasis and
574 macrophage function *in vivo*. We orthotopically implanted FC1245 WT, FC1245 WT
575 (*Cas9*) and FC1245$^{Msln-/-}$ (#4 and 6) cancer cells into the pancreas of syngeneic
576 immunocompetent mice (Fig. 5C and Supplementary Fig. S8A). We found that depletion
577 of mesothelin markedly reduced tumor growth and metastasis (Fig. 5D-F, Supplementary
578 Fig. S8B-C). Immunofluorescent staining for macrophages revealed that tumors lacking

mesothelin had significantly more MHC II+ macrophages, but fewer CD206+ and arginase+ macrophages in the primary PDAC tumors and lungs tissues (Fig. 5G, H, Supplementary Fig. S8D-E and S9A-D). The increase in MHC II+ macrophages in the FC1245$^{Msln-/-}$#4 and #6 tumors and lung was also confirmed by flow cytometry analysis (Supplementary Fig. S10A-D). Taken together, these results suggest that depletion of mesothelin leads to a reduction in tumor supporting macrophages in the FC1245$^{Msln-/-}$ PDAC tumors and lungs compared to the FC1245 WT tumors.

To establish whether mesothelin induces expression of VEGFA in macrophages we performed immunofluorescent staining of the primary tumors and lungs of mice bearing FC1245 WT or FC1245$^{Msln-/-}$ derived tumors. Genetic depletion of mesothelin in cancer cells reduced macrophage expression of VEGFA in both primary PDAC tumors and lungs (Fig. 6A-B and Supplementary Fig. S11A-B) but no changes in angiogenesis were observed (Fig. 6C and Supplementary Fig. S11C). We next investigated whether the reduction of macrophage VEGFA could impair cancer cell colony formation. As expected, cancer cells grown in the presence of conditioned media generated from exposure of macrophages to the FC1245$^{Msln-/-}$ #4 and #6 TCM, had a reduced colony forming ability compared to cancer cells grown in the presence of conditioned media generated from exposure of macrophages to the FC1245 WT TCM (Fig. 6D-E). Additionally, the growth of cancer cells exposed to the FC1245 WT Tumor educated Macrophage Conditioned Media (TeMCM) was inhibited by a VEGFR2 inhibitor. Taken together these data show that depletion of mesothelin leads to a decrease in macrophage-derived VEGFA and reduced cancer cell colony formation in a VEGFR2 dependent manner (Fig. 6D-E).

Next, we rescued mesothelin expression in the FC1245$^{Msln-/-}$ #4 cell line to generate the 'FC1245$^{Msln-/-}$ + *Msln'* cell line, and investigated whether rescue of mesothelin could increase tumor promoting functions of macrophages *in vitro* (Supplementary Fig. S6D-F). We confirmed the presence of mesothelin in the tumor conditioned media of the FC1245^{Msln} #4 cells by immunoblotting (Fig. 7A). Macrophages cultured with FC1245$^{Msln-/-}$

606 + *Msln* TCM showed a significant decrease in the ratio of MHC II+ : CD206 macrophages,
607 comparable to the macrophages cultures with the parental FC1245 WT TCMs (Fig. 7B).
608 Furthermore, reintroduction of mesothelin in cancer cells increased macrophage
609 expression of *Vegfa and S100a9* (Fig. 7C) and cancer cells exposed to those macrophage
610 secreted factors grow bigger colonies (Fig. 7D). Collectively, these data show that
611 mesothelin secretion from the cancer cells promotes the secretion of VEGFA by
612 macrophages which feedbacks to the cancer cells and supports their growth.

613 VEGFR2 is expressed on cancer cells in approximately 50-70% PDAC cases and its
614 presence on cancer cells correlates with a worse 5-year survival rate in stage IIa patients
615 (48). In agreement with the literature we also see variable VEGFR2 expression on cancer
616 cells in PDAC patient tissues (Supplementary Fig. S12A). We then set out to determine
617 whether PDAC patients with high mesothelin expression in tumor cells also had high levels
618 of VEGFA+ macrophages. We performed IF analysis on a subset of patients with low or
619 high MSLN expression and found that higher expression of mesothelin correlates with
620 significantly higher levels of VEGFA+/CD206+ macrophages (Supplementary Fig. S12B-
621 D). These data suggest that, similar to what we observed in mice, expression of mesothelin
622 by cancer cells in PDAC patients also promotes macrophage expression of VEGFA.

623 **Mesothelin triggers S100A9 expression by macrophages and promotes neutrophil**
624 **recruitment to the lungs and NET formation**

625 We next investigated macrophage expression of S100A9 in the tumors and lungs of mice
626 bearing FC1245 WT and FC1245$^{Msln-/-}$ tumors. Genetic depletion of cancer cell-derived
627 mesothelin did not affect macrophage expression of S100A9 in primary PDAC tumors (Fig.
628 8A and Supplementary Fig. S13A). However, there was a significant decrease in S100A9+
629 macrophages in the lungs from mice bearing FC1245$^{Msln-/-}$ tumors compared to the lungs
630 from mice bearing FC1245 WT tumors (Fig. 8B and Supplementary Fig. S13B).
631 Quantification of neutrophil abundance (Ly6G+) and NET formation (Ly6G+/Ci-H3+) in the
632 lungs revealed that there were significantly lower levels of Ly6G+ neutrophils in the lungs

633 from mice bearing FC1245$^{Msln-/-}$ tumors compared to the lungs from mice bearing FC1245
634 WT tumors (Fig. 8C and Supplementary Fig. S13C). The reduction in neutrophil
635 abundance was confirmed by flow cytometry analysis (Supplementary Fig. S13D).
636 Notably, genetic depletion of mesothelin also correlated with a decrease in neutrophil NET
637 formation in the lung and reduced PDAC lung metastasis (Fig. 8C).

638 **Differences in metastasis and macrophage populations are a function of mesothelin**
639 **expression and not tumor burden.**

640 Since cancer cells expressing high levels of mesothelin form both bigger primary tumors
641 and more metastases, we sought to determine whether the increase in metastasis is due
642 to the effect of mesothelin in macrophage function or whether it is a consequence of a
643 bigger tumor burden at the primary site. We compared FC1245 WT and FC1245$^{Msln-/-}$ #6
644 with similar primary tumor size from the *in vivo* experiments described in Fig. 5 and
645 Supplementary Fig. S8. We found that the FC1245 WT tumors produce significantly larger
646 lung metastases and metastasize more frequently to the lungs, livers and lymph nodes
647 compared to the FC1245$^{Msln-/-}$ #6 tumors, despite having a similar primary tumor burden
648 (Supplementary Fig. S14A-C). We also assessed macrophage phenotypes in the primary
649 tumors and lungs of these mice and found that the FC1245 WT PDAC tumors and lungs
650 had significantly more CD206+, arginase+ and VEGFA+ macrophages but less MHC II+
651 macrophages compared to the FC1245$^{Msln-/-}$ #6 tumors and lungs, which is consistent with
652 our previous findings (Supplementary Fig. S14D-G). Additionally, there were higher levels
653 of S100A9+ macrophages in the lungs but not in the primary tumors of mice bearing
654 FC1245 WT tumors compared to mice bearing FC1245$^{Msln-/-}$ #6, which is congruent with
655 our previous results. Therefore, these data suggest that the differences in PDAC
656 metastasis and macrophage phenotype are a function of mesothelin expression and not
657 of differences in primary tumor growth.

658

Discussion

In this study we sought to understand why PDAC cells of the same genetic background and with similar intrinsic capacity to proliferate and survive *in vitro* show different capacity to metastasize *in vivo*. We found that the secretion of the protein mesothelin by pancreatic cancer cells enhances PDAC tumor progression and metastasis. Mechanistically we reveal that mesothelin induces the conversion of macrophages towards a tumor supporting phenotype, capable of promoting metastasis via two distinct mechanisms, involving the secretion of VEGFA by macrophages which directly supports cancer cell survival and tumor growth, and the secretion of S100A9 which supports the recruitment of neutrophils and NET formation in the lung (Fig. 8D).

Research into the role of mesothelin in PDAC tumor progression and metastasis in pre-clinical models has been focused on human PDAC cell derived xenograft tumors implanted in immunocompromised mice to explore the therapeutic application of anti-human mesothelin blocking antibodies or immunotoxins (49-51). Only a few studies have evaluated the biological activity of mesothelin in immunocompetent mouse models of pancreatic cancer (52,53), and no study has assessed the role of secreted mesothelin in pancreatic cancer metastasis. Mesothelin was first reported to regulate macrophage function in the study by Dangaj *et al* where the authors showed that soluble mesothelin present in the ascites of ovarian cancer patients binds to CD206 on macrophages via its GPI-anchor and promotes the polarization of macrophages into immunosuppressive macrophages (31). More recently, mesothelin secreted by mesothelial cells was reported to support tissue resident large peritoneal macrophage (LPM) homeostasis by inducing expression of the GATA6 transcription factor in both embryonic derived and monocyte derived macrophages isolated from the mesothelium (32). The expression of GATA6 supports differentiation of large cavity macrophages (LPM) towards tissue repair, phagocytosis and an anti-inflammatory cytokine profile, while simultaneously downregulating MHCII, Gr1+ and costimulatory molecules CD80 and CD86 (54). Our

findings further support the notion that mesothelin regulates macrophage function but also provide new mechanistic insight of how mesothelin affects macrophage function and supports pancreatic cancer metastasis. Specifically, we find that mesothelin alters macrophage function to support metastasis by inducing macrophage expression of VEGFA and S100A9 leading to enhanced tumor growth and pro-metastatic NET formation in the lungs.

Cancer cell expression of mesothelin has been described to promote peritoneal metastasis in PDAC and ovarian cancers but the role of mesothelin in hematogenous or lymphatic routes of distant metastasis to the liver, lungs or lymph nodes was not known (51,55,56). Furthermore, the association of mesothelin expression to metastasis in cancer patients was unclear, with several studies providing evidence for (57-59) or against (57,60,61) the correlation of mesothelin expression to lymphatic or distant metastasis in several mesothelin expressing tumors. Here, we show that cancer cell secretion of mesothelin leads to a more aggressive disease by co-opting macrophages to support cancer metastasis. Our results exemplify mesothelin as a potential biomarker to predict PDAC patients at risk of metastasis. Our findings may apply to other mesothelin expressing solid cancers too, including mesothelioma, ovarian cancer, lung cancer and gastric cancer (57) and thus the pro-metastatic function of mesothelin we describe here may also be exploited in other solid cancers.

The expression of mesothelin on pancreatic cancer cells and dispensable mesothelial cells, but not healthy tissues makes it an attractive therapeutic target (33). A recent study reported that an anti-mesothelin monoclonal antibody could inhibit the transition of mesothelial cells into antigen presenting cancer associated fibroblasts (apCAF) in PDAC tumors (53). The decrease in apCAFs led to a decreased T reg/CD8+ T cell ratio and reduced tumor growth. Therefore, anti-mesothelin therapeutics may have synergistic effects by targeting tumor cells and inhibiting both tumor-promoting macrophage function and apCAF formation.

Mesothelin is a well-studied target for chimeric antigen receptor (CAR) T cell and NK cell therapies and a Listeria based vaccine in PDAC tumors (62,63) but neither have performed well in clinical trials. Significant barriers to immunotherapy in PDAC still remain, such as T cell trafficking and cytotoxic function in the fibrotic and immunosuppressive PDAC tumor microenvironment (64). However mesothelin CAR-T cells still hold promise, with several clinical trials using them in combination with anti-PD1 therapies (65). Notably, the study by Liu *et al* show that CAR T cells who bind adjacent to protease cleavage sites on mesothelin can inhibit shedding and improve anti-tumor immunity *in vivo* (66). Our data also suggest that mesothelin CAR-T cells could reduce metastatic outgrowth by not only targeting the cancer cells but also eliminating the source of secreted mesothelin and preventing pro-metastatic mesothelin-induced macrophage function.

We also observed that high expression of mesothelin in human PDAC tumors correlates with high levels of tumor promoting CD206+ macrophages expressing VEGFA. Anti-VEGFA therapies have shown mixed success in clinical trials in the past two decades. The anti-VEGFA monoclonal antibody bevacizumab has been successful in treating several metastatic solid tumors, such as renal cell carcinoma, colorectal cancer and glioblastoma, but has failed in pancreatic cancer among other cancers (67). However, there is renewed interest for combining anti-VEGF therapies with immunotherapy for their ability to normalize tumor vasculature, relieve VEGF mediated immunosuppression and to improve trafficking of anti-tumor immune cell populations into PDAC tumors (68). Our data suggest that mesothelin secretion by pancreatic cancer cells increases macrophage expression of VEGFA and S100A9 which could be used as potential biomarkers to highlight patients who may benefit from a combination of anti-VEGF and/or anti-S100A9 combined with immunotherapies.

Cancer cell expression of mesothelin has been linked to increased activation of ERK1/2 and AKT signaling pathways and results in increased cancer cell proliferation and survival, resistance to anoikis *in vitro* and chemoresistance *in vivo* in several preclinical models of

cancer (69-71). Expression of mesothelin also promotes cancer cell EMT, invasion and migration *in vitro* (33,72) and increases metastasis in xenograft in vivo models *(70,71)*. However, in our study, mesothelin did not alter cancer cell intrinsic proliferation, survival or EMT. Similar to our findings, the knockout of mesothelin in KLM1 pancreatic cancer cells in the study by Avula *et al* show no changes in cancer cell intrinsic proliferation *in vitro* (55).

A limitation of our findings is that we have not been able to demonstrate whether the GPI-anchored form of secreted mesothelin was responsible for macrophage polarization. Mesothelin may also be cleaved upstream of the GPI anchor by sheddase enzymes (73). Additional studies may seek to utilize truncated mesothelin (31), site-directed mutagenesis of the GPI anchor transaminase cleavage site required for GPI anchor linking (74) or CRISPR knockout of GPI anchor biosynthesis enzymes (75) to study the requirement of GPI-anchor in mesothelin induced macrophage polarization.

References

1. National Cancer Registration and Analysis Service: Stage Breakdown by CCG 2017 [cited 2023 February 15]. Available from http://www.ncin.org.uk/publications/survival_by_stage
2. Kleeff J, Korc M, Apte M, La Vecchia C, Johnson CD, Biankin AV*, et al.* Pancreatic cancer. Nature reviews Disease primers **2016**;2:16022
3. Haeno H, Gonen M, Davis MB, Herman JM, Iacobuzio-Donahue CA, Michor F. Computational modeling of pancreatic cancer reveals kinetics of metastasis suggesting optimum treatment strategies. Cell **2012**;148:362-75
4. Matsumoto I, Murakami Y, Shinzeki M, Asari S, Goto T, Tani M*, et al.* Proposed preoperative risk factors for early recurrence in patients with resectable pancreatic ductal adenocarcinoma after surgical resection: A multi-center retrospective study. Pancreatology **2015**;15:674-80
5. Neoptolemos JP, Stocken DD, Friess H, Bassi C, Dunn JA, Hickey H*, et al.* A randomized trial of chemoradiotherapy and chemotherapy after resection of pancreatic cancer. The New England journal of medicine **2004**;350:1200-10
6. Iacobuzio-Donahue CA, Fu B, Yachida S, Luo M, Abe H, Henderson CM*, et al.* DPC4 gene status of the primary carcinoma correlates with patterns of failure in patients with

pancreatic cancer. Journal of clinical oncology : official journal of the American Society of Clinical Oncology **2009**;27:1806-13

7. Van den Broeck A, Sergeant G, Ectors N, Van Steenbergen W, Aerts R, Topal B. Patterns of recurrence after curative resection of pancreatic ductal adenocarcinoma. Eur J Surg Oncol **2009**;35:600-4

8. Rhim AD, Mirek ET, Aiello NM, Maitra A, Bailey JM, McAllister F*, et al.* EMT and dissemination precede pancreatic tumor formation. Cell **2012**;148:349-61

9. Yachida S, White CM, Naito Y, Zhong Y, Brosnan JA, Macgregor-Das AM*, et al.* Clinical significance of the genetic landscape of pancreatic cancer and implications for identification of potential long-term survivors. Clinical cancer research : an official journal of the American Association for Cancer Research **2012**;18:6339-47

10. Hessmann E, Buchholz SM, Demir IE, Singh SK, Gress TM, Ellenrieder V*, et al.* Microenvironmental Determinants of Pancreatic Cancer. Physiol Rev **2020**;100:1707-51

11. Ireland LV, Mielgo A. Macrophages and Fibroblasts, Key Players in Cancer Chemoresistance. Front Cell Dev Biol **2018**;6:131

12. Yang S, Liu Q, Liao Q. Tumor-Associated Macrophages in Pancreatic Ductal Adenocarcinoma: Origin, Polarization, Function, and Reprogramming. Front Cell Dev Biol **2020**;8:607209

13. Quaranta V, Rainer C, Nielsen SR, Raymant ML, Ahmed MS, Engle DD*, et al.* Macrophage-Derived Granulin Drives Resistance to Immune Checkpoint Inhibition in Metastatic Pancreatic Cancer. Cancer Res **2018**;78:4253-69

14. Ginhoux F, Schultze JL, Murray PJ, Ochando J, Biswas SK. New insights into the multidimensional concept of macrophage ontogeny, activation and function. Nat Immunol **2016**;17:34-40

15. Zhu Y, Herndon JM, Sojka DK, Kim KW, Knolhoff BL, Zuo C*, et al.* Tissue-Resident Macrophages in Pancreatic Ductal Adenocarcinoma Originate from Embryonic Hematopoiesis and Promote Tumor Progression. Immunity **2017**;47:323-38.e6

16. Ireland L, Santos A, Ahmed MS, Rainer C, Nielsen SR, Quaranta V*, et al.* Chemoresistance in Pancreatic Cancer Is Driven by Stroma-Derived Insulin-Like Growth Factors. Cancer Res **2016**;76:6851-63

17. Ireland L, Santos A, Campbell F, Figueiredo C, Hammond D, Ellies LG*, et al.* Blockade of insulin-like growth factors increases efficacy of paclitaxel in metastatic breast cancer. Oncogene **2018**;37:2022-36

18. Nielsen SR, Quaranta V, Linford A, Emeagi P, Rainer C, Santos A*, et al.* Macrophage-secreted granulin supports pancreatic cancer metastasis by inducing liver fibrosis. Nat Cell Biol **2016**;18:549-60

19. Quail DF, Joyce JA. Microenvironmental regulation of tumor progression and metastasis. Nature medicine **2013**;19:1423-37
20. Mielgo A, Schmid MC. Liver Tropism in Cancer: The Hepatic Metastatic Niche. Cold Spring Harb Perspect Med **2020**;10
21. Bellomo G, Rainer C, Quaranta V, Astuti Y, Raymant M, Boyd E*, et al.* Chemotherapy-induced infiltration of neutrophils promotes pancreatic cancer metastasis via Gas6/AXL signalling axis. Gut **2022**;71:2284-99
22. Ireland L, Luckett T, Schmid MC, Mielgo A. Blockade of Stromal Gas6 Alters Cancer Cell Plasticity, Activates NK Cells, and Inhibits Pancreatic Cancer Metastasis. Front Immunol **2020**;11:297
23. Xiao Y, Cong M, Li J, He D, Wu Q, Tian P*, et al.* Cathepsin C promotes breast cancer lung metastasis by modulating neutrophil infiltration and neutrophil extracellular trap formation. Cancer cell **2021**;39:423-37 e7
24. Liu Y, Gu Y, Han Y, Zhang Q, Jiang Z, Zhang X*, et al.* Tumor Exosomal RNAs Promote Lung Pre-metastatic Niche Formation by Activating Alveolar Epithelial TLR3 to Recruit Neutrophils. Cancer cell **2016**;30:243-56
25. Li R, Wen A, Lin J. Pro-Inflammatory Cytokines in the Formation of the Pre-Metastatic Niche. Cancers (Basel) **2020**;12
26. Wang D, Sun H, Wei J, Cen B, DuBois RN. CXCL1 Is Critical for Premetastatic Niche Formation and Metastasis in Colorectal Cancer. Cancer Res **2017**;77:3655-65
27. Peran I, Madhavan S, Byers SW, McCoy MD. Curation of the Pancreatic Ductal Adenocarcinoma Subset of the Cancer Genome Atlas Is Essential for Accurate Conclusions about Survival-Related Molecular Mechanisms. Clinical cancer research : an official journal of the American Association for Cancer Research **2018**;24:3813-9
28. Perez-Riverol Y, Bai J, Bandla C, Garcia-Seisdedos D, Hewapathirana S, Kamatchinathan S*, et al.* The PRIDE database resources in 2022: a hub for mass spectrometry-based proteomics evidences. Nucleic Acids Res **2022**;50:D543-D52
29. Hu H, Tu W, Chen Y, Zhu M, Jin H, Huang T*, et al.* The combination of PKM2 overexpression and M2 macrophages infiltration confers a poor prognosis for PDAC patients. Journal of Cancer **2020**;11:2022-31
30. Patterson MT, Burrack AL, Xu Y, Hickok GH, Schmiechen ZC, Becker S*, et al.* Tumor-specific CD4 T cells instruct monocyte fate in pancreatic ductal adenocarcinoma. Cell Rep **2023**;42:112732
31. Dangaj D, Abbott KL, Mookerjee A, Zhao A, Kirby PS, Sandaltzopoulos R*, et al.* Mannose receptor (MR) engagement by mesothelin GPI anchor polarizes tumor-associated macrophages and is blocked by anti-MR human recombinant antibody. PloS one **2011**;6:e28386

32. Lai CW, Bagadia P, Barisas DAG, Jarjour NN, Wong R, Ohara T*, et al.* Mesothelium-Derived Factors Shape GATA6-Positive Large Cavity Macrophages. Journal of immunology (Baltimore, Md : 1950) **2022**;209:742-50
33. Shimizu A, Hirono S, Tani M, Kawai M, Okada K, Miyazawa M*, et al.* Coexpression of MUC16 and mesothelin is related to the invasion process in pancreatic ductal adenocarcinoma. Cancer science **2012**;103:739-46
34. Lauc G, Heffer-Lauc M. Shedding and uptake of gangliosides and glycosylphosphatidylinositol-anchored proteins. Biochimica et biophysica acta **2006**;1760:584-602
35. Rodriguez PC, Zea AH, DeSalvo J, Culotta KS, Zabaleta J, Quiceno DG*, et al.* L-arginine consumption by macrophages modulates the expression of CD3 zeta chain in T lymphocytes. Journal of immunology (Baltimore, Md : 1950) **2003**;171:1232-9
36. Oberlies J, Watzl C, Giese T, Luckner C, Kropf P, Muller I*, et al.* Regulation of NK cell function by human granulocyte arginase. Journal of immunology (Baltimore, Md : 1950) **2009**;182:5259-67
37. Lichtenberger BM, Tan PK, Niederleithner H, Ferrara N, Petzelbauer P, Sibilia M. Autocrine VEGF signaling synergizes with EGFR in tumor cells to promote epithelial cancer development. Cell **2010**;140:268-79
38. Ma F, Zhang B, Ji S, Hu H, Kong Y, Hua Y*, et al.* Hypoxic Macrophage-Derived VEGF Promotes Proliferation and Invasion of Gastric Cancer Cells. Dig Dis Sci **2019**;64:3154-63
39. Goel HL, Mercurio AM. VEGF targets the tumour cell. Nature reviews Cancer **2013**;13:871-82
40. Peng H, Zhang Q, Li J, Zhang N, Hua Y, Xu L*, et al.* Apatinib inhibits VEGF signaling and promotes apoptosis in intrahepatic cholangiocarcinoma. Oncotarget **2016**;7:17220-9
41. Koch S, Claesson-Welsh L. Signal transduction by vascular endothelial growth factor receptors. Cold Spring Harb Perspect Med **2012**;2:a006502
42. Simard JC, Girard D, Tessier PA. Induction of neutrophil degranulation by S100A9 via a MAPK-dependent mechanism. Journal of leukocyte biology **2010**;87:905-14
43. Adrover JM, McDowell SAC, He XY, Quail DF, Egeblad M. NETworking with cancer: The bidirectional interplay between cancer and neutrophil extracellular traps. Cancer cell **2023**
44. Hiratsuka S, Watanabe A, Aburatani H, Maru Y. Tumour-mediated upregulation of chemoattractants and recruitment of myeloid cells predetermines lung metastasis. Nat Cell Biol **2006**;8:1369-75

45. Wu CF, Andzinski L, Kasnitz N, Kroger A, Klawonn F, Lienenklaus S*, et al.* The lack of type I interferon induces neutrophil-mediated pre-metastatic niche formation in the mouse lung. Int J Cancer **2015**;137:837-47
46. Kinoshita R, Sato H, Yamauchi A, Takahashi Y, Inoue Y, Sumardika IW*, et al.* Newly developed anti-S100A8/A9 monoclonal antibody efficiently prevents lung tropic cancer metastasis. Int J Cancer **2019**;145:569-75
47. Park J, Wysocki RW, Amoozgar Z, Maiorino L, Fein MR, Jorns J*, et al.* Cancer cells induce metastasis-supporting neutrophil extracellular DNA traps. Science translational medicine **2016**;8:361ra138
48. Doi Y, Yashiro M, Yamada N, Amano R, Ohira G, Komoto M*, et al.* Significance of phospho-vascular endothelial growth factor receptor-2 expression in pancreatic cancer. Cancer science **2010**;101:1529-35
49. Mizukami T, Kamachi H, Fujii Y, Matsuzawa F, Einama T, Kawamata F*, et al.* The anti-mesothelin monoclonal antibody amatuximab enhances the anti-tumor effect of gemcitabine against mesothelin-high expressing pancreatic cancer cells in a peritoneal metastasis mouse model. Oncotarget **2018**;9:33844-52
50. Fujii Y, Kamachi H, Matsuzawa F, Mizukami T, Kobayashi N, Fukai M*, et al.* Early administration of amatuximab, a chimeric high-affinity anti-mesothelin monoclonal antibody, suppresses liver metastasis of mesothelin-expressing pancreatic cancer cells and enhances gemcitabine sensitivity in a xenograft mouse model. Invest New Drugs **2021**;39:1256-66
51. Coelho R, Ricardo S, Amaral AL, Huang YL, Nunes M, Neves JP*, et al.* Regulation of invasion and peritoneal dissemination of ovarian cancer by mesothelin manipulation. Oncogenesis **2020**;9:61
52. Zervos E, Agle S, Freistaedter AG, Jones GJ, Roper RL. Murine mesothelin: characterization, expression, and inhibition of tumor growth in a murine model of pancreatic cancer. J Exp Clin Cancer Res **2016**;35:39
53. Huang H, Wang Z, Zhang Y, Pradhan RN, Ganguly D, Chandra R*, et al.* Mesothelial cell-derived antigen-presenting cancer-associated fibroblasts induce expansion of regulatory T cells in pancreatic cancer. Cancer cell **2022**;40:656-73 e7
54. Honda M, Kadohisa M, Yoshii D, Komohara Y, Hibi T. Directly recruited GATA6 + peritoneal cavity macrophages contribute to the repair of intestinal serosal injury. Nat Commun **2021**;12:7294
55. Avula LR, Rudloff M, El-Behaedi S, Arons D, Albalawy R, Chen X*, et al.* Mesothelin Enhances Tumor Vascularity in Newly Forming Pancreatic Peritoneal Metastases. Molecular Cancer Research **2019**

56. Matsuzawa F, Kamachi H, Mizukami T, Einama T, Kawamata F, Fujii Y*, et al.* Mesothelin blockage by Amatuximab suppresses cell invasiveness, enhances gemcitabine sensitivity and regulates cancer cell stemness in mesothelin-positive pancreatic cancer cells. BMC Cancer **2021**;21:200
57. Weidemann S, Gagelmann P, Gorbokon N, Lennartz M, Menz A, Luebke AM*, et al.* Mesothelin Expression in Human Tumors: A Tissue Microarray Study on 12,679 Tumors. Biomedicines **2021**;9
58. Cristaudo A, Foddis R, Vivaldi A, Guglielmi G, Dipalma N, Filiberti R*, et al.* Clinical significance of serum mesothelin in patients with mesothelioma and lung cancer. Clinical cancer research : an official journal of the American Association for Cancer Research **2007**;13:5076-81
59. Cheng WF, Huang CY, Chang MC, Hu YH, Chiang YC, Chen YL*, et al.* High mesothelin correlates with chemoresistance and poor survival in epithelial ovarian carcinoma. British journal of cancer **2009**;100:1144-53
60. Suzuki T, Yamagishi Y, Einama T, Koiwai T, Yamasaki T, Fukumura-Koga M*, et al.* Membrane mesothelin expression positivity is associated with poor clinical outcome of luminal-type breast cancer. Oncol Lett **2020**;20:193
61. Inoue S, Tsunoda T, Riku M, Ito H, Inoko A, Murakami H*, et al.* Diffuse mesothelin expression leads to worse prognosis through enhanced cellular proliferation in colorectal cancer. Oncol Lett **2020**;19:1741-50
62. Yeo D, Giardina C, Saxena P, Rasko JEJ. The next wave of cellular immunotherapies in pancreatic cancer. Mol Ther Oncolytics **2022**;24:561-76
63. Le DT, Picozzi VJ, Ko AH, Wainberg ZA, Kindler H, Wang-Gillam A*, et al.* Results from a Phase IIb, Randomized, Multicenter Study of GVAX Pancreas and CRS-207 Compared with Chemotherapy in Adults with Previously Treated Metastatic Pancreatic Adenocarcinoma (ECLIPSE Study). Clinical cancer research : an official journal of the American Association for Cancer Research **2019**;25:5493-502
64. Akce M, Zaidi MY, Waller EK, El-Rayes BF, Lesinski GB. The Potential of CAR T Cell Therapy in Pancreatic Cancer. Front Immunol **2018**;9:2166
65. Zhai X, Mao L, Wu M, Liu J, Yu S. Challenges of Anti-Mesothelin CAR-T-Cell Therapy. Cancers (Basel) **2023**;15
66. Liu X, Onda M, Watson N, Hassan R, Ho M, Bera TK*, et al.* Highly active CAR T cells that bind to a juxtamembrane region of mesothelin and are not blocked by shed mesothelin. Proceedings of the National Academy of Sciences of the United States of America **2022**;119:e2202439119

67. Garcia J, Hurwitz HI, Sandler AB, Miles D, Coleman RL, Deurloo R*, et al.* Bevacizumab (Avastin(R)) in cancer treatment: A review of 15 years of clinical experience and future outlook. Cancer Treat Rev **2020**;86:102017
68. An YF, Pu N, Jia JB, Wang WQ, Liu L. Therapeutic advances targeting tumor angiogenesis in pancreatic cancer: Current dilemmas and future directions. Biochim Biophys Acta Rev Cancer **2023**;1878:188958
69. Zheng C, Jia W, Tang Y, Zhao H, Jiang Y, Sun S. Mesothelin regulates growth and apoptosis in pancreatic cancer cells through p53-dependent and -independent signal pathway. J Exp Clin Cancer Res **2012**;31:84
70. Li M, Bharadwaj U, Zhang R, Zhang S, Mu H, Fisher WE*, et al.* Mesothelin is a malignant factor and therapeutic vaccine target for pancreatic cancer. Molecular cancer therapeutics **2008**;7:286-96
71. He X, Wang L, Riedel H, Wang K, Yang Y, Dinu CZ*, et al.* Mesothelin promotes epithelial-to-mesenchymal transition and tumorigenicity of human lung cancer and mesothelioma cells. Mol Cancer **2017**;16:63
72. Chang MC, Chen CA, Chen PJ, Chiang YC, Chen YL, Mao TL*, et al.* Mesothelin enhances invasion of ovarian cancer by inducing MMP-7 through MAPK/ERK and JNK pathways. The Biochemical journal **2012**;442:293-302
73. Liu X, Chan A, Tai CH, Andresson T, Pastan I. Multiple proteases are involved in mesothelin shedding by cancer cells. Commun Biol **2020**;3:728
74. Gíslason MH, Nielsen H, Almagro Armenteros JJ, Johansen AR. Prediction of GPI-anchored proteins with pointer neural networks. Current Research in Biotechnology **2021**;3:6-13
75. Hagel KR, Arafeh R, Gang S, Arnoff TE, Larson RC, Doench JG*, et al.* Systematic Interrogation of Tumor Cell Resistance to Chimeric Antigen Receptor T-cell Therapy in Pancreatic Cancer. Cancer Res **2023**;83:613-25

Acknowledgements

We would like to thank David Tuveson for his kind donation of the KPC-derived cancer cell lines. We also would like to acknowledge the histology facility, proteomics facility, flow cytometry facility, biomedical services unit and pre-clinical imaging facility for their provision of technical assistance and equipment. We thank Patrick Freeman for his help with termination of the *in vivo* experiment and with the collection of human PDAC tissues. We would like to acknowledge the feedback provided by all members of the Mielgo and Schmid labs. We thank the gastro-histopathologists Tim Andrews, Susanne Burdak-

Rothkamm, Susan Macpherson and Manal Atwan for their help with collection and histological diagnoses of human pancreatic cancer samples. We also would like to thank the patients, who consented for the collection of pancreatic cancer samples used in this study.

These studies were supported by grants from North West Cancer Research (CR1194) and Wellcome Trust (102521/Z/13/Z) for A.M., Cancer Research UK (A25607, A26978), Medical Research Council (MR/P018920/1) for M.C.S

Author Contributions

TL designed and performed most of the experiments, analyzed and interpreted the data. TL also performed the bioinformatics analysis for this study. LI performed the proteomic/secretome experiment. LI and TL analyzed the proteomic secretome data. MA assisted TL with FACS analysis and performed IF/IHC staining for the knockout out *in vivo* studies. MG designed the experimental protocol for the CRISPR knockout of mesothelin and helped TL with the generation of CRISPR knockout clones and the rescue experiment. GB performed surgery for the *in vivo* mesothelin knockout studies. RS, RJ, PG, CH provided patient samples. MS provided conceptual advice and interpreted the data. TL and AM wrote the manuscript. AM provided conceptual advice, designed experiments, interpreted the data, conceived and supervised the project. All authors critically analyzed and approved the manuscript.

Competing Interests

The authors declare no competing interests.

Figure 1 – Metastatic pancreatic tumors have higher numbers of CD206+/MHCII- tumor associated macrophages compared to low metastatic tumors. (A) Schematic

illustrating orthotopic implantation of FC1199 or FC1245 pancreatic cancer cell lines that stably express *zsGreen*/*luciferase,* into the pancreas of recipient syngeneic C57BL/6 mice. At day 20 the tumors, livers, lungs and mesenteric lymph nodes were harvested for analysis. **(B)** Tumor weights at day 20. (FC1199 n=8, FC1245 n=7). Data shown are mean±SD. **(C)** Representative images of metastatic burden using bioluminescent imaging (BLI). **(D)** *Ex vivo* quantification of metastatic burden using BLI imaging. Data are mean±SD. **(E)** MTT assay for *in vitro* cancer cell proliferation. **(F)** Colony formation assay for cells grown in 3D culture. Data are mean±SEM from 6 independent experiments. **(G)** mRNA expression levels of EMT inducting transcription factors: *Snail1, Snail2, Twist1, Twist2, Zeb1, Zeb2*; epithelial markers: *Cdh1* (E-cadherin), *Ctnnb1* (β-catenin), *Epcam*; mesenchymal markers *Vim (*Vimentin), *Cdh2* (n-cadherin) in FC1199 and FC1245 cancer cells grown *in vitro*. Data shown are from 3 independent experiments, mean ±SEM. **(H)** Representative immunofluorescent images and quantification of proliferating cells (Ki67+) and cancer cells (CK19+) in primary PDAC tumors. **(I)** Representative immunofluorescent images and quantification of apoptotic cells (TUNEL+) and cancer cells (CK19+) in PDAC tumors using TUNEL assay. Data are mean ±SEM. **(J-K)** Representative immunofluorescent (IF) images and quantification of MHC II+ / F4/80+ and CD206+ / F480+ macrophages in the primary tumor **(J)** and lung tissues **(K)**. Scale bars are 100µM. Unpaired t-test was performed to calculate P values. *P<0.05, **P<0.01, ***P<0.001.

Figure 2 – Secretome analysis identifies mesothelin as a top candidate highly expressed by metastatic pancreatic cancer cells that correlate with an increase in CD206+ macrophages and worse prognosis in PDAC patients. (A) Stable Isotope labelling by amino acids in cell culture (SILAC) secretome analysis experiment schematic and stratification criteria. A total of 4 secretome replicates were performed for each cell line. **(B)** Volcano plot of differentially secreted proteins. P value cut off is 0.01 and Log2 fold change (FC) cut off is 1.25. **(C)** Survival analysis of proteins enriched or exclusive to the high metastatic (FC1245) TCM using The Cancer Genome Atlas (TGCA) data. Kaplan-

Meier p-values are plotted against hazard ratios. P value cut off = 0.05. **(D)** Immunoblotting and densitometry analysis for mesothelin present in the tumor conditioned media (TCM) of the FC1199 and FC1245 cancer cell lines standardized to total protein detected by ponceau stain. **(E)** mRNA expression levels of *Gpld1* in FC1199 and FC1245 cancer cells. Data are from 3 independent experiments, mean±SEM. **(F)** Immunoblotting for GPI-specific phospholipase D (GPI-PLD) in the protein lysates of FC1199 and FC1245 cells. **(G)** Representative immunohistochemical images of mesothelin and CD206 in serial sections from human PDAC tissues. Yellow arrows denote ductal structures analyzed for MSLN staining. Red arrows denote positive staining for CD206. Scale bar 100µM. **(H)** Linear regression analysis of mesothelin staining intensity on ductal cancer cells scored 1 (low) to 5 (high) plotted against number of CD206+ cells (per 3-8 fields of view. n=25 human PDAC samples). Unpaired t-test was used to calculate P values. *P<0.05, **P<0.01, ***P<0.001.

Figure 3 – Mesothelin secretion correlates with an increase in macrophages that express *arginase*, *S100A9* and *VEGFA*. (A) Experiment schematic and expression levels of macrophage genes (*Ciita*, *Cd86, Nos2, Tnfa, Il1b, Cxcl10Mrc1, Arg1, Il6, Chil3, Tgfb1, Gas6, Mmp9, Il10, S100a8, S100a9, Pcdc1lg1, Vegfa*) in primary bone marrow derived macrophages cultured *in vitro and* exposed to tumor conditioned media (TCM) from low metastatic FC1199 or high metastatic FC1245 cancer cells. Data are shown as fold change compared to FC1199 TCM from each independent experiment. Data are from 3 independent experiments, mean±SEM. **(B-D)** Representative IF images and quantification of Arginase+ / F4/80+ macrophages **(B)**, VEGFA+ / F4/80+ macrophages **(C)** and S100A9+ / F4/80+ macrophages **(D)** in PDAC primary tumors and lungs of mice with low metastatic FC1199-dervied tumors (n=8) or high metastatic FC1245-derived tumors. Yellow arrows denote double positive staining. Data are mean±SEM. Scale bars are 100µM. Unpaired t-test was used to calculate P values. P*<0.05, P**<0.01, P***<0.001.

Figure 4 - Macrophages exposed to high metastatic (FC1245) TCM support cancer cell growth and neutrophil NETosis. (A) Representative images and quantification of endothelial cell micro vessel density (MVD) using immunohistochemistry staining of CD31 in PDAC tumors. (FC1199 n=8, FC1245 n=7). Data are mean ±SEM**. (B)** Schematic for colony formation assay experiment. **(C)** Colony formation assay (CFA) for cancer cells cultured in the presence of low metastatic FC1199 or high metastatic FC1245 Tumor educated Macrophage Conditioned Media (TeMCM). Representative brightfield images of the colonies are shown. Data are mean±SEM from 3 independent experiments. **(D)** Immunoblotting and densitometry analysis for phosphorylated-VEGFR2, total VEGFR2 and α-tubulin in the protein lysates from high metastatic (FC1245) cells ± recombinant-VEGFA and ± VEGFR2 inhibitor (Ki8751). Media +20% FBS was used a positive control. **(E)** Colony formation assay (CFA) for FC1245 cancer cells exposed to either FC1199 or FC1245 TeMCM, ±DMSO or ±VEGFR2 inhibitor (Ki8751). Representative brightfield images of the colonies are shown. Data are mean±SEM from 3 independent experiments. **(F)** Colony formation assay of low metastatic (FC1199) and high metastatic (FC1245) cancer cells treated with recombinant-VEGFA (150ng/ml). Representative brightfield images of the colonies are shown. Quantification of colony formation performed with BLI. Data are from 3 independent experiments, mean±SEM. **(G)** Immunofluorescent staining for neutrophil marker, LyG6, in FC1199 and FC1245 PDAC tumors. Data are mean±SEM. **(H)** Representative IF images and quantification of NETs formed by neutrophils (Ly6G+) using NETosis marker citrullinated histone H3 (Ci-H3) in the lungs of mice with FC1199 or FC1245 tumors. Yellow arrows denote double positive staining. Data are mean±SEM. All scale bars are 100μM. Unpaired t-test was used to calculate P values. P*<0.05, P**<0.01, P***<0.001.

Figure 5 – Knockout of mesothelin in the high metastatic (FC1245) cancer cells reduces tumor growth, metastatic burden and alters macrophage function. (A) Immunoblotting for mesothelin (MSLN) in the TCM of FC1245 WT, single cell cloned FC1245^{Cas9} WT and FC1245$^{Msln-/-}$ clones #4 and #6. **(B)** Representative IF images and quantification of the ratio of MHC II+: CD206+ macrophages cultured with TCM from FC1245 WT, FC1245 WT (*Cas9)* or FC1245$^{Msln-/-}$ #4 and #6 cells. Data are from 3 independent experiments, mean±SEM. **(C)** Schematic illustrating orthotopic implantation of FC1245 WT, FC1245^{Cas9} WT or FC1245$^{Msln-/-}$ #4 and #6 pancreatic cancer cell lines that stably express *zsGreen*/*luciferase,* into the pancreas of recipient syngeneic C57BL/6 mice and grown until day 20. The tumors, livers, lungs and mesenteric tumor draining lymph nodes were harvested for metastatic burden quantification. The tumors and lungs from half of the mice were analyzed by IF/IHC whereas the remaining half were digested for flow cytometry analysis. **(D)** Tumor weights at day 20. FC1245 WT (n= 8), FC1245^{Cas9} WT, FC1245$^{Msln-/-}$ #4 (n=8) and FC1245$^{Msln-/-}$ #6 (n=8). Data are mean±SD. **(E)** Representative images of metastatic burden using bioluminescent imaging (BLI). **(F)** *Ex vivo* quantification of metastatic burden using BLI. Data represents mean±SD. One-way ANOVA with Kruskal-Wallis multiple comparison test was used to calculate adjusted P values. **(G** and **H)** Representative IFs images and quantification of MHC II+ / F4/80+ macrophages and CD206+ / F4/80+ macrophages in primary PDAC tumors **(G)** and lungs **(H)**. Data are mean±SEM. Scale bars are 100µM. One-way ANOVA with Šidák multiple comparison test was used to calculate adjusted P values. *P<0.05, **P<0.01, ***P<0.001.

Figure 6 – Cancer cell secretion of mesothelin induces macrophage expression of *Vegfa* to enhance tumor growth and cancer cell colony formation in a VEGFR2 dependent manner. (A and B) Representative images and quantification of VEGFA+ / F4/80+ macrophages in FC1245 WT (n= 8), FC1245 WT (*Cas9*), FC1245$^{Msln-/-}$ #4 (n=8) and #6 (n=8) derived PDAC tumors **(A)** and lungs **(B).** Yellow arrows denote double

positive cells. Data are mean±SEM. **(C)** Representative images and quantification of endothelial cell micro vessel density (MVD) using immunohistochemistry staining of CD31 in FC1245 WT and FC1245$^{Msln-/-}$ PDAC tumors. **(D)** Colony formation assay schematic. **(E)** Colony formation assay for cancer cells grown in the presence of high metastatic FC1245 WT, FC1245^{Cas9} WT, FC1245$^{Msln-/-}$ #4 and #6 TeMCM, ±DMSO and ±VEGFR2 inhibitor (Ki8751). Representative brightfield images of the colonies are shown. Quantification of colony formation performed with BLI following administration of luciferin. Data are from 3 independent experiments shown as mean±SEM. Scale bars are 100µM. One-way ANOVA with Šidák multiple comparison test was used to calculate adjusted P values. *P<0.05, **P<0.01, ***P<0.001.

Figure 7 – Rescue of mesothelin expression in the FC1245$^{Msln-/-}$ #4 increases tumor promoting macrophage function. (A) Immunoblot for secreted mesothelin in the TCM of FC1245 WT, FC1245^{Cas9} WT, FC1245$^{Msln-/-}$ #4 and FC1245$^{Msln-/-}$ + *Msln* cells. **(B)** Immunofluorescent staining of macrophages cultured with FC1245 WT, FC1245 WT (*Cas9*), FC1245$^{Msln-/-}$ #4 and FC1245$^{Msln-/-}$ + *Msln* TCM. **(C)** Expression of *Vegfa* and *S100A9* in macrophages cultured with TCM from FC1245 WT, FC1245 WT (*Cas9)*, FC1245$^{Msln-/-}$ and FC1245$^{Msln-/-}$ + *Msln* cells. Data are from 3 independent experiments, mean±SEM. **(D)** Colony formation assay for cancer cells grown in the presence of conditioned media generated from macrophages (TeMCM) exposed to FC1245 WT, FC1245^{Cas9} WT, FC1245$^{Msln-/-}$ #4 and FC1245$^{Msln-/-}$ + *Msln* TeMCM. Representative brightfield images of the colonies are shown. Quantification of colony formation performed with BLI following administration of luciferin. Data are from 3 independent experiments shown as mean±SEM. One-way ANOVA with Šidák multiple comparison test was used to calculate adjusted P values. *P<0.05, **P<0.01, ***P<0.001.

Figure 8 – Tumors expressing mesothelin have increased levels of S100A9+ macrophages, neutrophil infiltrate and NET formation in lungs.

(A and **B)** Representatives images and quantification of F4/80+ / S100A9+ macrophages in the PDAC tumour **(A)** lungs **(B)** from mice bearing FC1245 or FC1245$^{Msln-/-}$ tumors**.** Data are mean±SEM. **(C)** Representative IF images and quantification of NETs formed by neutrophils (Ly6G+) using the NETosis marker citrullinated histone H3 (Ci-H3) in the lungs of mice bearing FC1245 WT or FC1245$^{Msln-/-}$ tumors. Data are mean±SEM. Yellow arrows denote double positive cells. Scale bars are 100µM. One-way ANOVA with Šidák multiple comparison test was used to generate adjusted P values. *P<0.05, **P<0.01, ***P<0.001. **(D)** Schematic depicting how mesothelin secreted by pancreatic cancer cells regulates macrophage tumor supporting functions leading to increased tumor growth and metastasis.

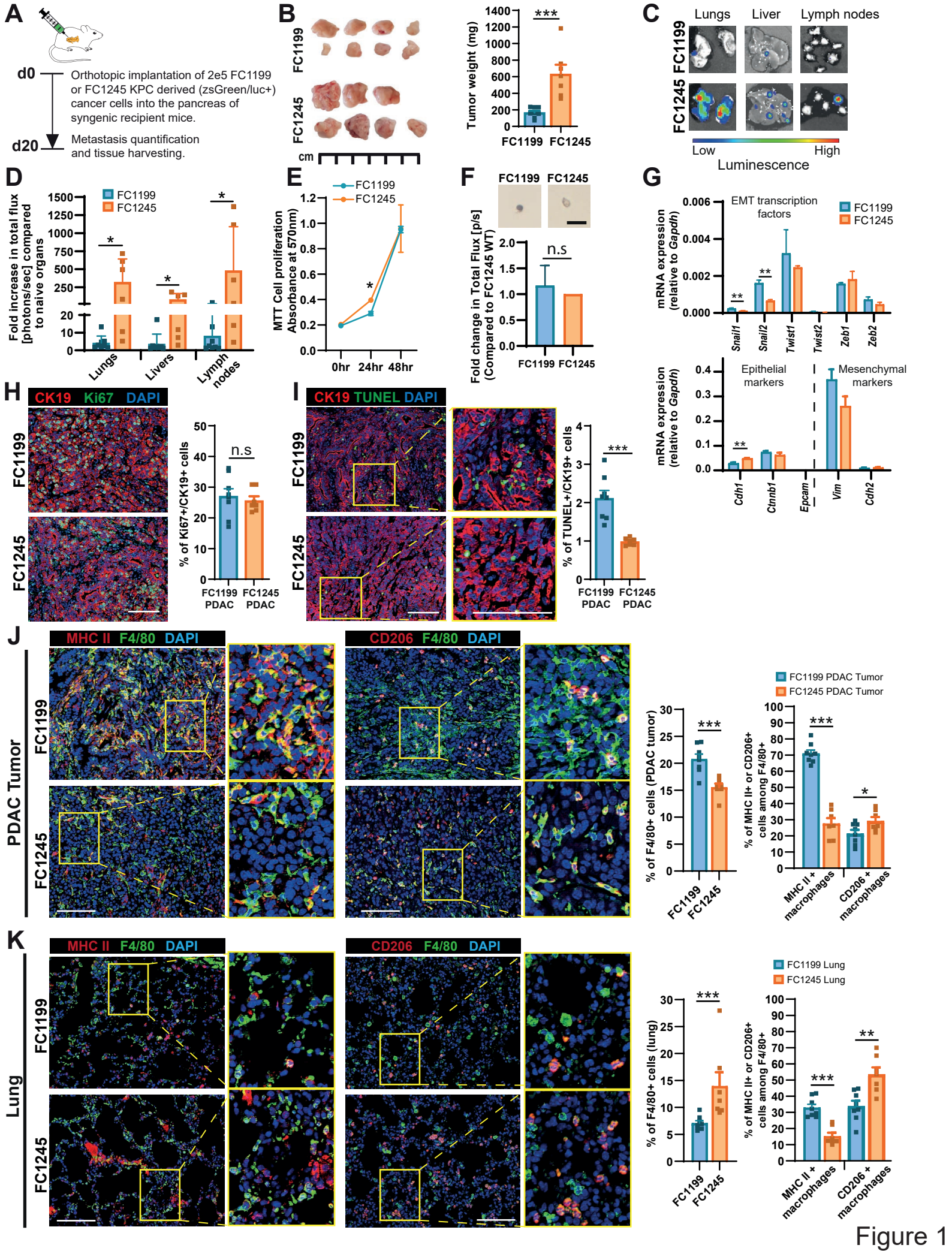
A
d0
Orthotopic implantation of 2e5 FC1199 or FC1245 KPC derived (zsGreen/luc+) cancer cells into the pancreas of syngenic recipient mice.
d20
Metastasis quantification and tissue harvesting.
B
FC1199
FC1245
cm
Tumor weight (mg)
***
FC1199 FC1245
C
Lungs
Liver
Lymph nodes
FC1199
FC1245
Low
High
Luminescence
D
Fold increase in total flux [photons/sec] compared to naive organs
FC1199
FC1245
Lungs
Livers
Lymph nodes
E
MTT Cell proliferation Absorbance at 570nm)
0hr 24hr 48hr
F
Fold change in Total Flux [p/s] (Compared to FC1245 WT)
n.s
G
mRNA expression (relative to Gapdh)
EMT transcription factors
Snail1 Snail2 Twist1 Twist2 Zeb1 Zeb2
Epithelial markers
Mesenchymal markers
Cdh1 Ctnnb1 Epcam Vim Cdh2
H
CK19 Ki67 DAPI
% of Ki67+/CK19+ cells
n.s
FC1199 PDAC
FC1245 PDAC
I
CK19 TUNEL DAPI
% of TUNEL+/CK19+ cells
J
PDAC Tumor
MHC II F4/80 DAPI
CD206 F4/80 DAPI
% of F4/80+ cells (PDAC tumor)
FC1199 PDAC Tumor
FC1245 PDAC Tumor
% of MHC II+ or CD206+ cells among F4/80+
MHC II + macrophages
CD206 + macrophages
K
Lung
MHC II F4/80 DAPI
CD206 F4/80 DAPI
% of F4/80+ cells (lung)
FC1199 Lung
FC1245 Lung

Figure 1

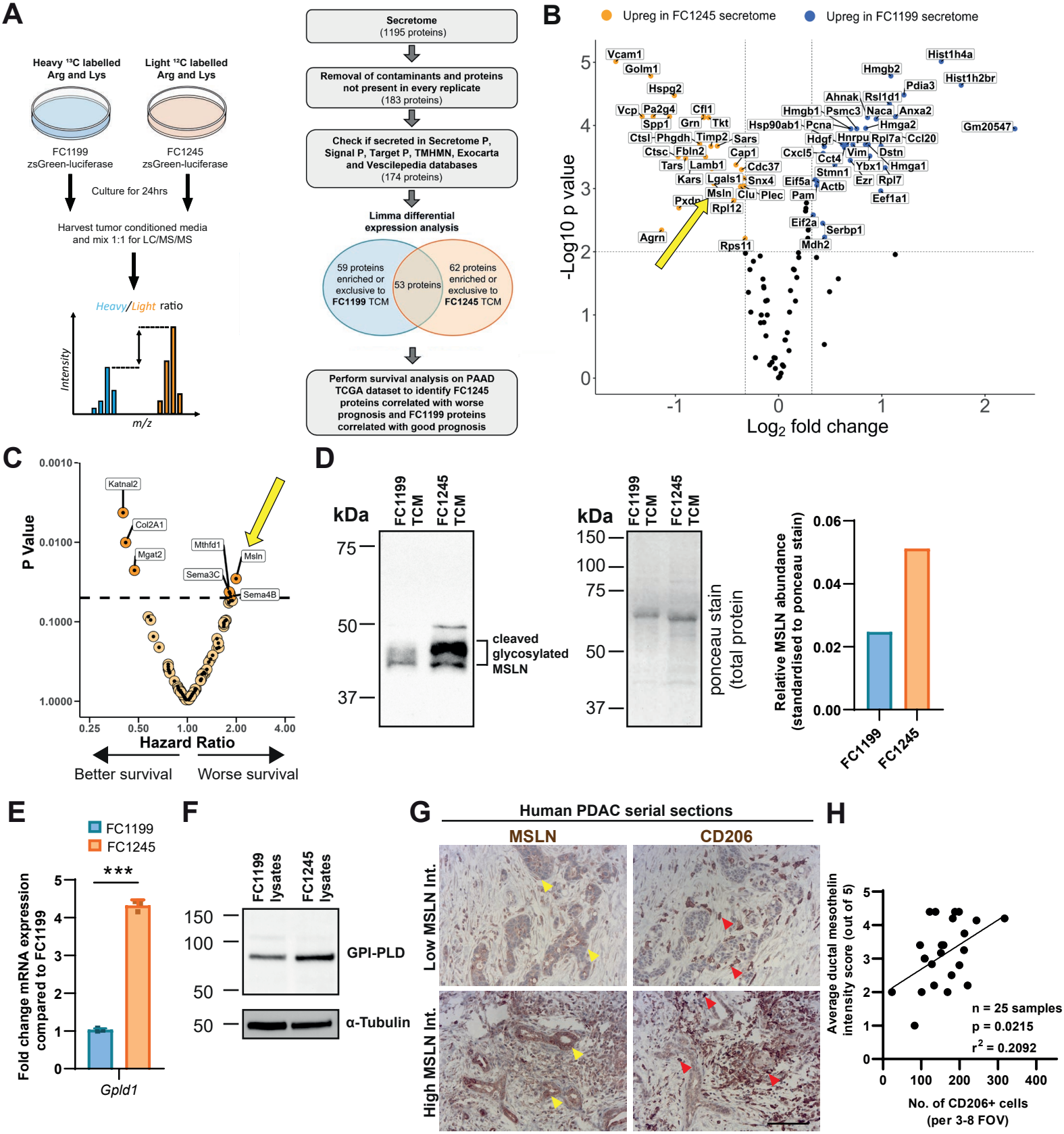
A
Heavy ¹³C labelled Arg and Lys
Light ¹²C labelled Arg and Lys
FC1199 zsGreen-luciferase
FC1245 zsGreen-luciferase
Culture for 24hrs
Harvest tumor conditioned media and mix 1:1 for LC/MS/MS
Heavy/Light ratio
Intensity
m/z
Secretome (1195 proteins)
Removal of contaminants and proteins not present in every replicate (183 proteins)
Check if secreted in Secretome P, Signal P, Target P, TMHMM, Exocarta and Vescilepedia databases (174 proteins)
Limma differential expression analysis
59 proteins enriched or exclusive to FC1199 TCM
53 proteins
62 proteins enriched or exclusive to FC1245 TCM
Perform survival analysis on PAAD TCGA dataset to identify FC1245 proteins correlated with worse prognosis and FC1199 proteins correlated with good prognosis
B
Upreg in FC1245 secretome
Upreg in FC1199 secretome
-Log10 p value
Log2 fold change
C
P Value
Katnal2
Col2A1
Mgat2
Mthfd1
Msln
Sema3C
Sema4B
Hazard Ratio
Better survival
Worse survival
D
kDa
FC1199 TCM
FC1245 TCM
cleaved glycosylated MSLN
ponceau stain (total protein
Relative MSLN abundance (standardised to ponceau stain)
E
FC1199
FC1245
***
Fold change mRNA expression compared to FC1199
Gpld1
F
FC1199 lysates
FC1245 lysates
GPI-PLD
α-Tubulin
G
Human PDAC serial sections
MSLN
CD206
Low MSLN Int.
High MSLN Int.
H
Average ductal mesothelin intensity score (out of 5)
n = 25 samples
p = 0.0215
r² = 0.2092
No. of CD206+ cells (per 3-8 FOV)

Figure 2

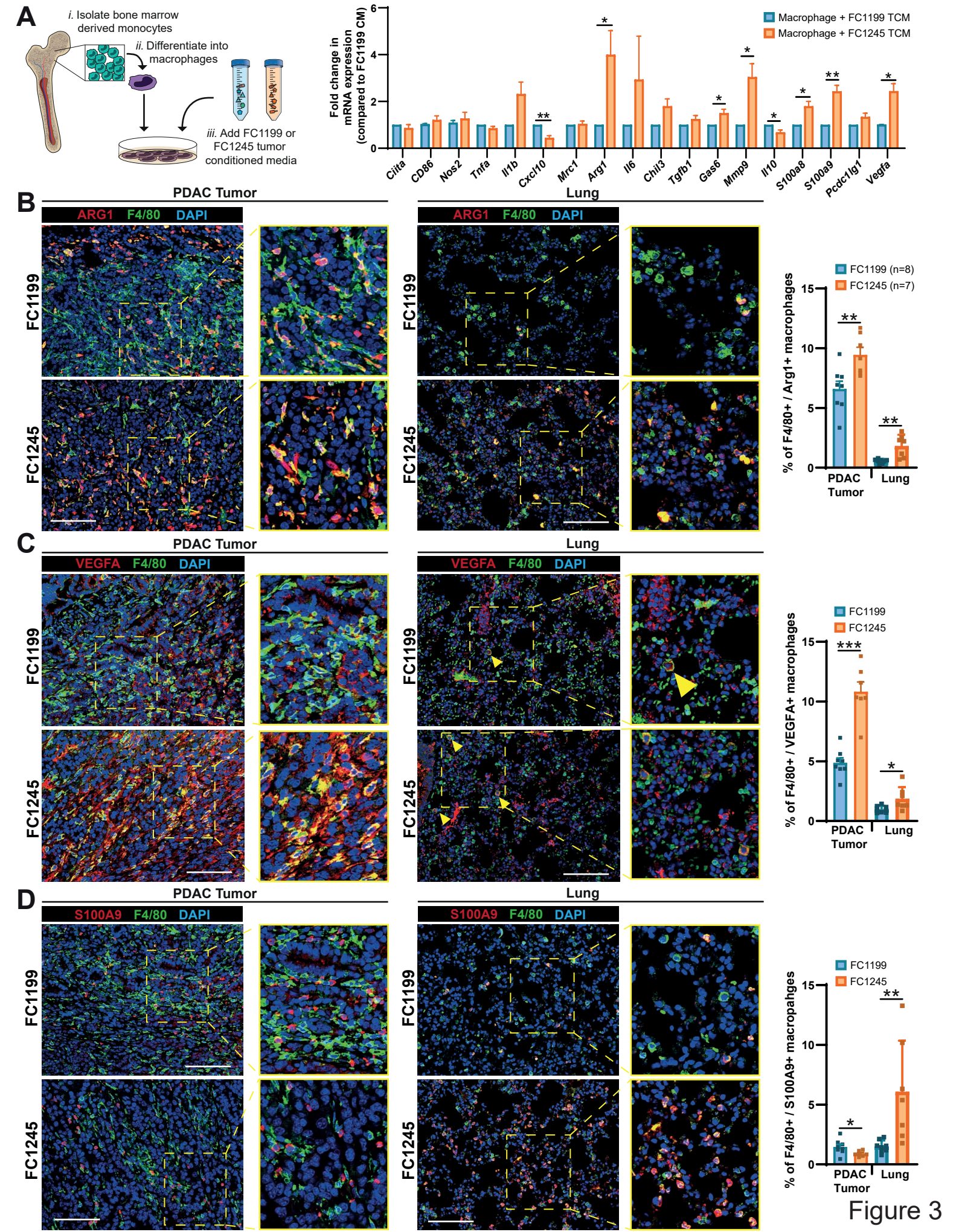
A
i. Isolate bone marrow derived monocytes
ii. Differentiate into macrophages
iii. Add FC1199 or FC1245 tumor conditioned media
Fold change in mRNA expression (compared to FC1199 CM)
Macrophage + FC1199 TCM
Macrophage + FC1245 TCM
Ciita
CD86
Nos2
Tnfa
Il1b
Cxcl10
Mrc1
Arg1
Il6
Chil3
Tgfb1
Gas6
Mmp9
Il10
S100a8
S100a9
Pcdc1lg1
Vegfa
B
PDAC Tumor
Lung
ARG1 F4/80 DAPI
FC1199
FC1245
% of F4/80+ / Arg1+ macrophages
FC1199 (n=8)
FC1245 (n=7)
PDAC Tumor
Lung
C
VEGFA F4/80 DAPI
% of F4/80+ / VEGFA+ macrophages
D
S100A9 F4/80 DAPI
% of F4/80+ / S100A9+ macropahges

Figure 3

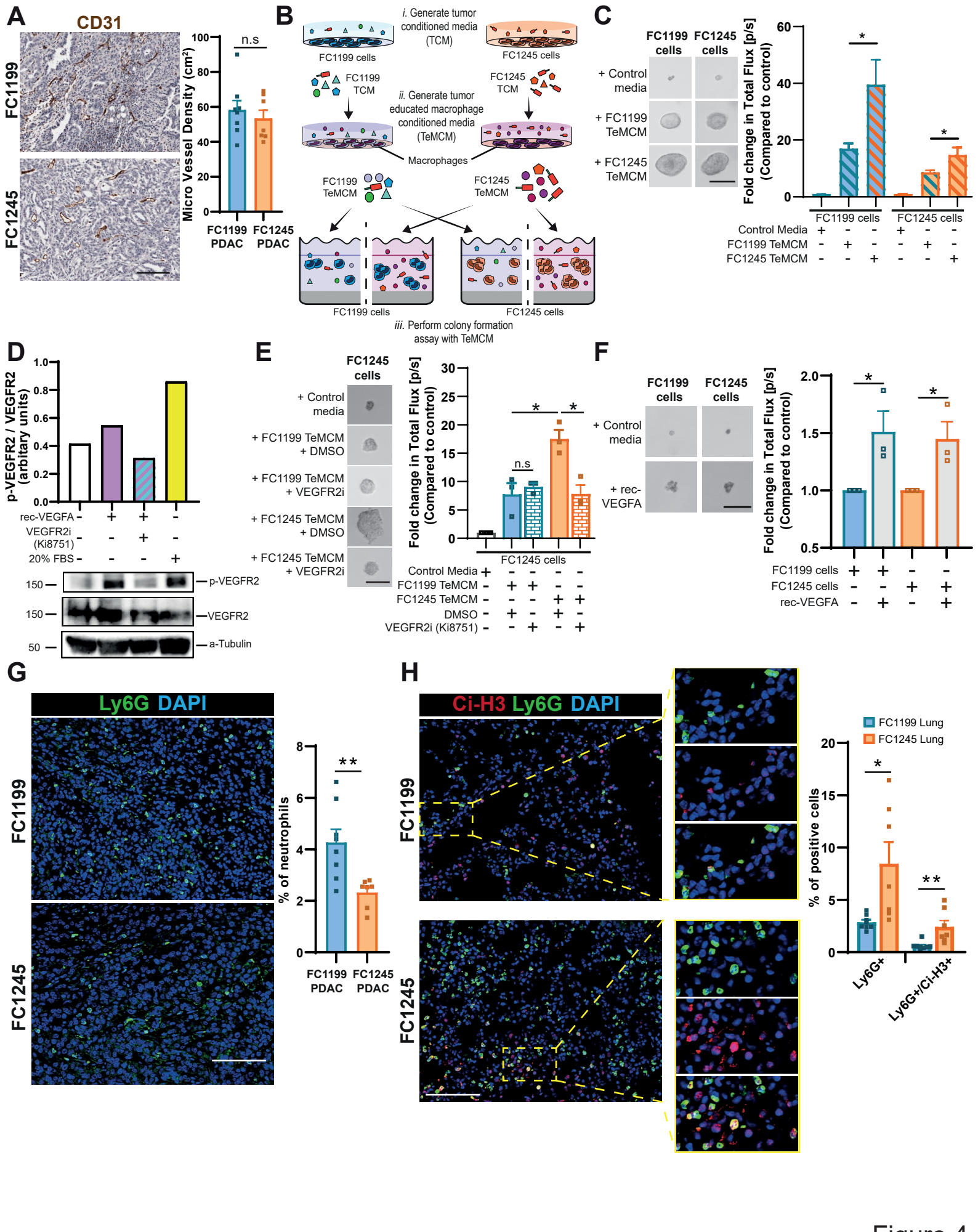
A
CD31
FC1199
FC1245
Micro Vessel Density (cm²)
n.s
FC1199 PDAC
FC1245 PDAC
B
i. Generate tumor conditioned media (TCM)
FC1199 cells
FC1245 cells
FC1199 TCM
FC1245 TCM
ii. Generate tumor educated macrophage conditioned media (TeMCM)
Macrophages
FC1199 TeMCM
FC1245 TeMCM
FC1199 cells
FC1245 cells
iii. Perform colony formation assay with TeMCM
C
FC1199 cells
FC1245 cells
+ Control media
+ FC1199 TeMCM
+ FC1245 TeMCM
Fold change in Total Flux [p/s] (Compared to control)
FC1199 cells
FC1245 cells
Control Media
FC1199 TeMCM
FC1245 TeMCM
D
p-VEGFR2 / VEGFR2 (arbitary units)
rec-VEGFA
VEGFR2i (Ki8751)
20% FBS
150
p-VEGFR2
150
VEGFR2
50
a-Tubulin
E
FC1245 cells
+ Control media
+ FC1199 TeMCM + DMSO
+ FC1199 TeMCM + VEGFR2i
+ FC1245 TeMCM + DMSO
+ FC1245 TeMCM + VEGFR2i
Fold change in Total Flux [p/s] (Compared to control)
n.s
FC1245 cells
Control Media
FC1199 TeMCM
FC1245 TeMCM
DMSO
VEGFR2i (Ki8751)
F
FC1199 cells
FC1245 cells
+ Control media
+ rec-VEGFA
Fold change in Total Flux [p/s] (Compared to control)
FC1199 cells
FC1245 cells
rec-VEGFA
G
Ly6G DAPI
FC1199
FC1245
% of neutrophils
FC1199 PDAC
FC1245 PDAC
H
Ci-H3 Ly6G DAPI
FC1199
FC1245
FC1199 Lung
FC1245 Lung
% of positive cells
Ly6G+
Ly6G+/Ci-H3+

Figure 4

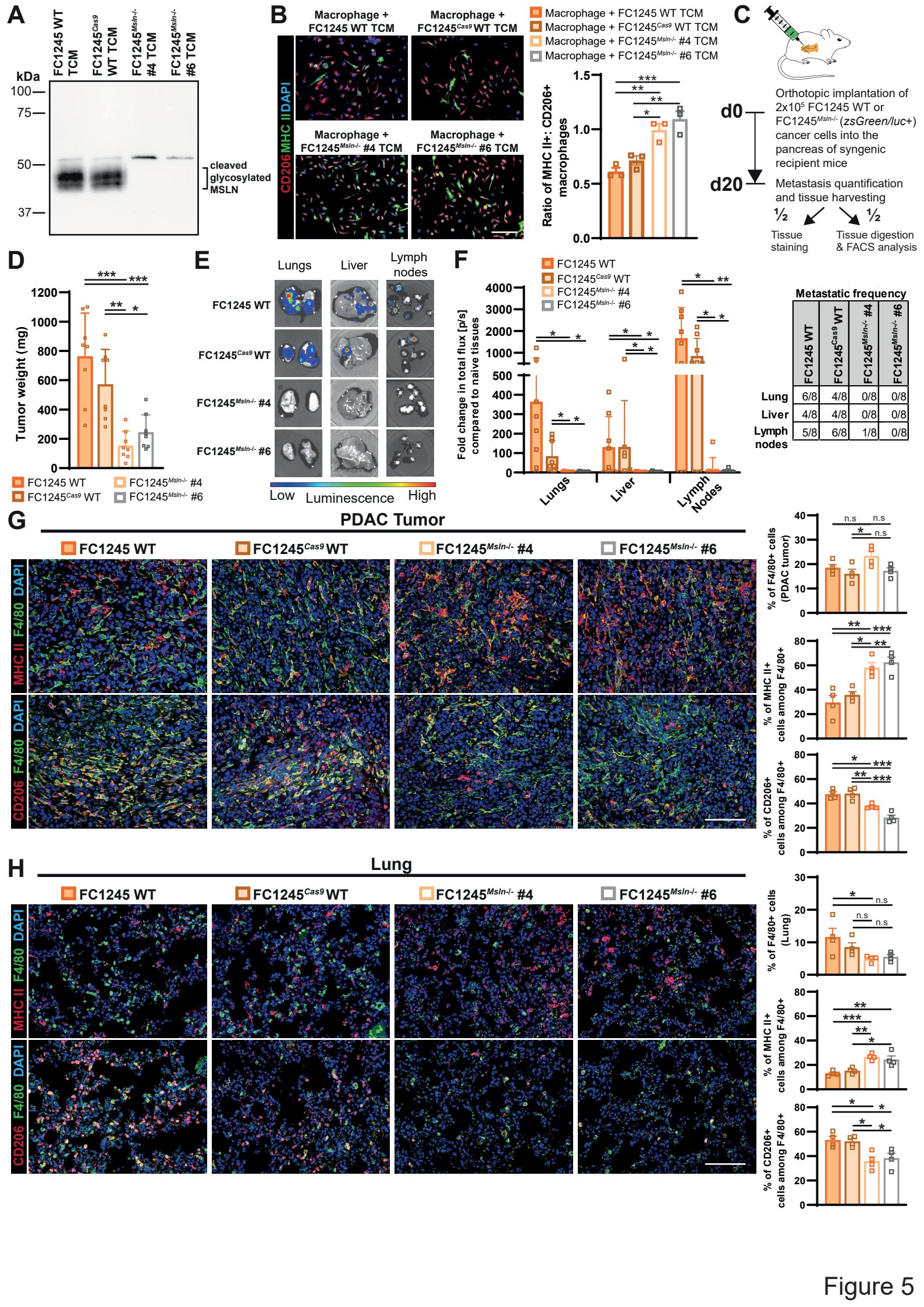
A
FC1245 WT TCM
FC1245Cas9 WT TCM
FC1245Msln-/- #4 TCM
FC1245Msln-/- #6 TCM
kDa
100
75
50
37
cleaved glycosylated MSLN
B
Macrophage + FC1245 WT TCM
Macrophage + FC1245Cas9 WT TCM
Macrophage + FC1245Msln-/- #4 TCM
Macrophage + FC1245Msln-/- #6 TCM
CD206 MHC II DAPI
Ratio of MHC II+: CD206+ macrophages
C
Orthotopic implantation of 2x10⁵ FC1245 WT or FC1245Msln-/- (zsGreen/luc+) cancer cells into the pancreas of syngenic recipient mice
d0
d20
Metastasis quantification and tissue harvesting
½
Tissue staining
½
Tissue digestion & FACS analysis
D
Tumor weight (mg)
FC1245 WT
FC1245Cas9 WT
FC1245Msln-/- #4
FC1245Msln-/- #6
E
Lungs
Liver
Lymph nodes
Low
Luminescence
High
F
Fold change in total flux [p/s] compared to naive tissues
Lungs
Liver
Lymph Nodes
Metastatic frequency
Lung 6/8 4/8 0/8 0/8
Liver 4/8 4/8 0/8 0/8
Lymph nodes 5/8 6/8 1/8 0/8
G
PDAC Tumor
MHC II F4/80 DAPI
CD206 F4/80 DAPI
% of F4/80+ cells (PDAC tumor)
% of MHC II+ cells among F4/80+
% of CD206+ cells among F4/80+
H
Lung
% of F4/80+ cells (Lung)
% of MHC II+ cells among F4/80+
% of CD206+ cells among F4/80+

Figure 5

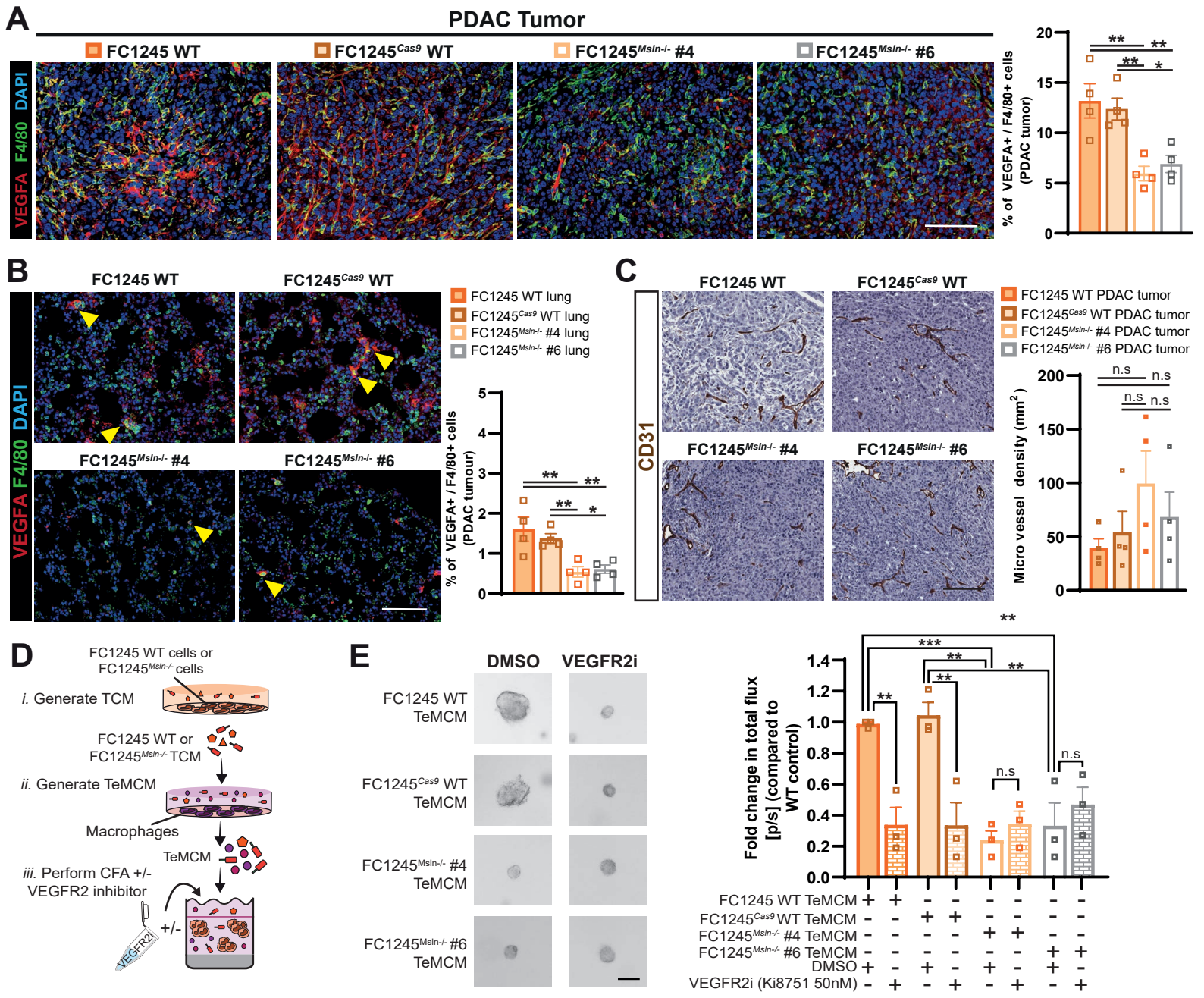
A
PDAC Tumor
FC1245 WT
FC1245Cas9 WT
FC1245Msln-/- #4
FC1245Msln-/- #6
VEGFA F4/80 DAPI
% of VEGFA+ / F4/80+ cells (PDAC tumor)
B
FC1245 WT
FC1245Cas9 WT
FC1245Msln-/- #4
FC1245Msln-/- #6
VEGFA F4/80 DAPI
FC1245 WT lung
FC1245Cas9 WT lung
FC1245Msln-/- #4 lung
FC1245Msln-/- #6 lung
% of VEGFA+ / F4/80+ cells (PDAC tumour)
C
CD31
FC1245 WT PDAC tumor
FC1245Cas9 WT PDAC tumor
FC1245Msln-/- #4 PDAC tumor
FC1245Msln-/- #6 PDAC tumor
Micro vessel density (mm2)
n.s
D
FC1245 WT cells or FC1245Msln-/- cells
i. Generate TCM
FC1245 WT or FC1245Msln-/- TCM
ii. Generate TeMCM
Macrophages
TeMCM
iii. Perform CFA +/- VEGFR2 inhibitor
VEGFR2i
+/-
E
DMSO
VEGFR2i
FC1245 WT TeMCM
FC1245Cas9 WT TeMCM
FC1245Msln-/- #4 TeMCM
FC1245Msln-/- #6 TeMCM
Fold change in total flux [p/s] (compared to WT control)
FC1245 WT TeMCM
FC1245Cas9 WT TeMCM
FC1245Msln-/- #4 TeMCM
FC1245Msln-/- #6 TeMCM
DMSO
VEGFR2i (Ki8751 50nM)

Figure 6

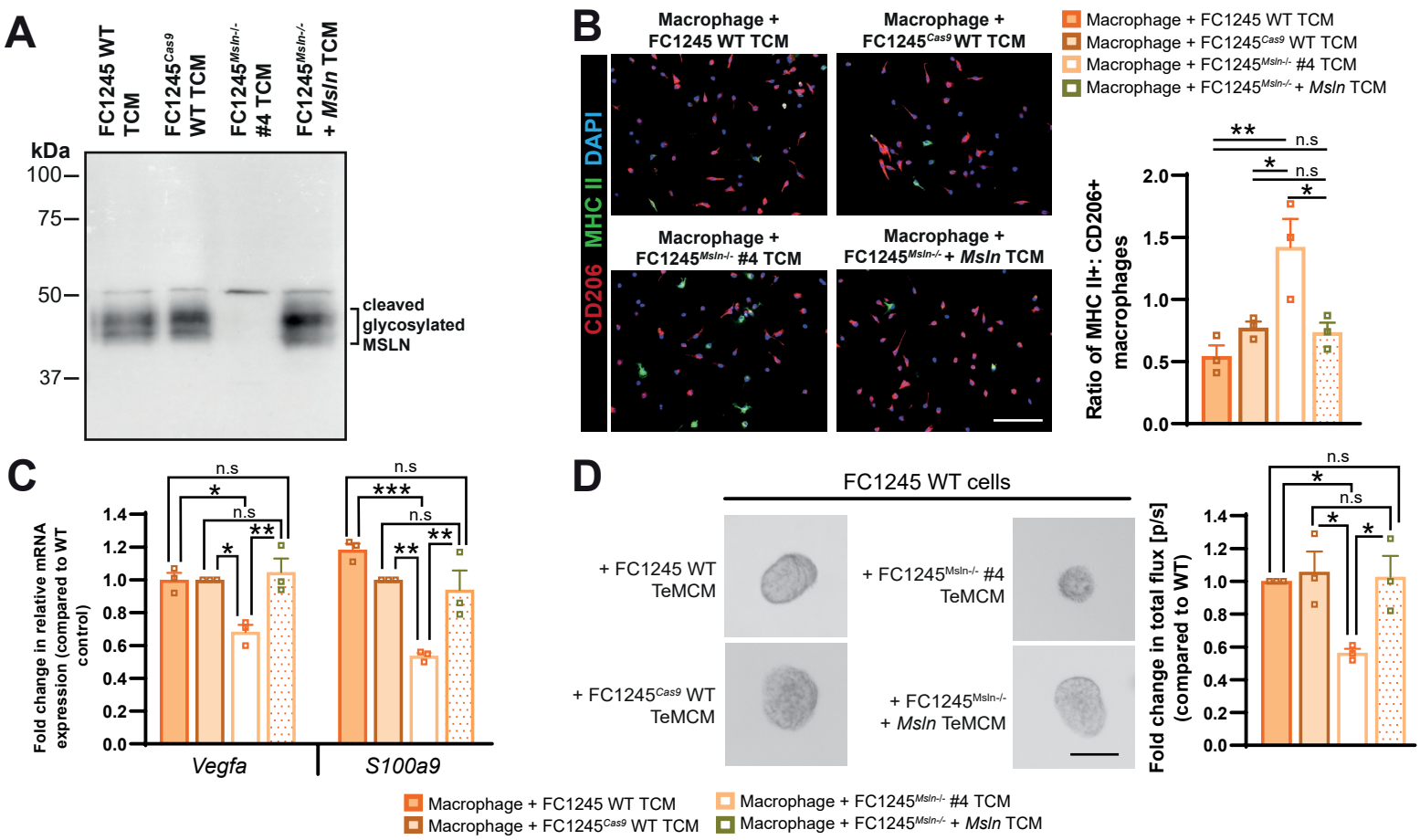
A
FC1245 WT TCM
FC1245Cas9 WT TCM
FC1245Msln-/- #4 TCM
FC1245Msln-/- + Msln TCM
kDa
100
75
50
37
cleaved glycosylated MSLN
B
Macrophage + FC1245 WT TCM
Macrophage + FC1245Cas9 WT TCM
Macrophage + FC1245Msln-/- #4 TCM
Macrophage + FC1245Msln-/- + Msln TCM
CD206 MHC II DAPI
Ratio of MHC II+: CD206+ macrophages
n.s
C
Fold change in relative mRNA expression (compared to WT control)
Vegfa
S100a9
D
FC1245 WT cells
+ FC1245 WT TeMCM
+ FC1245Msln-/- #4 TeMCM
+ FC1245Cas9 WT TeMCM
+ FC1245Msln-/- + Msln TeMCM
Fold change in total flux [p/s] (compared to WT)

Figure 7

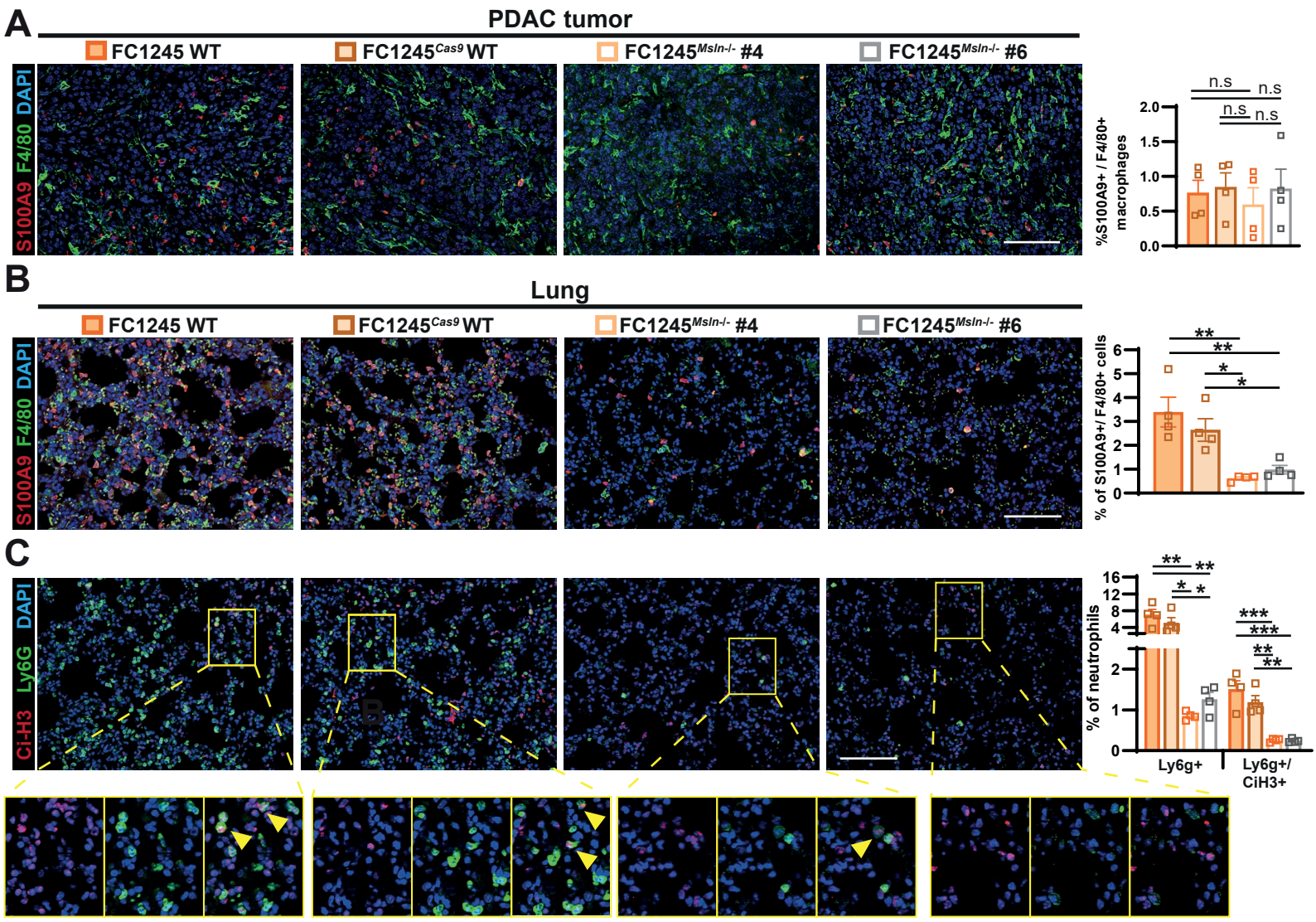
A
PDAC tumor
FC1245 WT
FC1245Cas9 WT
FC1245Msln-/- #4
FC1245Msln-/- #6
S100A9 F4/80 DAPI
%S100A9+ / F4/80+ macrophages
n.s
B
Lung
% of S100A9+/ F4/80+ cells
C
Ly6G Ci-H3 DAPI
% of neutrophils
Ly6g+
Ly6g+/ CiH3+

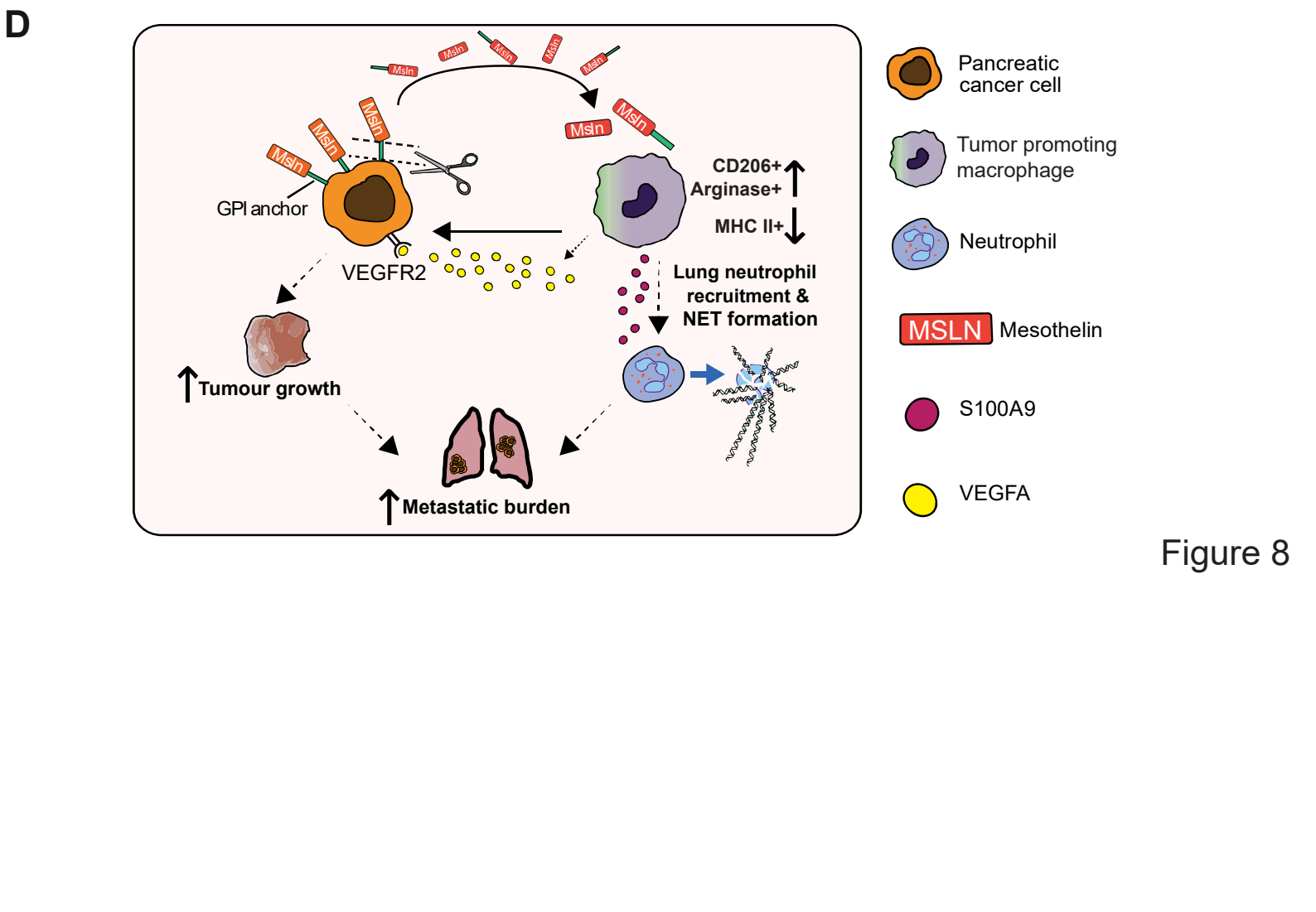
D
Msln
GPI anchor
VEGFR2
CD206+
Arginase+
MHC II+
Lung neutrophil recruitment & NET formation
Tumour growth
Metastatic burden
Pancreatic cancer cell
Tumor promoting macrophage
Neutrophil
MSLN Mesothelin
S100A9
VEGFA

Figure 8